ACES Asian Chemical Editorial Society

doi.org/10.1002/cnma.202400629

CHEMNANOMAT
Review

www.chemnanomat.org

Porous Organic Framework Membranes with Nanostructures for Osmotic Power Conversion, Water Desalination, and Selective Separation

Lixue Yang, Zhe Wang,* Zhong Lin Wang,* and Di Wei*

Nanostructured porous organic framework (POF) membranes have gained recognition as leading contenders for osmotic-related applications due to their exceptional selectivity and permeability. Recent years have witnessed significant progress in the fabrication of nanostructured POF membranes, such as metal–organic frameworks, covalent organic frameworks, and hydrogen-bonded organic frameworks. These nanostructured membranes exhibit pore sizes on the angstrom scale, which is commensurate with the kinetic diameters of ions and small molecules. They also possess low thicknesses—down to mere nanometers—and offer tunable structures and functional groups that further optimize both selectivity and permeability. In this review, recent advancements in the fabrication methods of advanced nanostructured POF membranes are summarized. In addition, we will highlight and discuss in detail emerging osmotic applications of these nanostructured porous organic membranes, including osmotic power conversion, water desalination, and selective separation. Finally, future development and challenges of nanostructured porous organic membranes are also summarized.

1. Introduction

Membranes, as a revolutionary separation materials, have fundamentally redefined traditional separation and filtration methods through their highly efficient selective permeability and distinct separation mechanisms, offering more energy-efficient, environmentally sustainable, and effective solutions.[1,2] In response to increasing demand, researchers have dedicated extensive efforts to developing advanced membrane materials aimed at further enhancing selective permeability and ion transport performance of membrane processes,[3] for example, polymer membranes,[4] alumina membranes,[5] graphene oxide (GO) membranes,[6,7] nanofiber membranes,[8] zeolite-polymer membranes,[9] ion exchange membranes,[10,11] and porous organic framework (POF) membranes,[12–14] all of which have been utilized across various separation technologies. At the same time, the application scope of these membranes continues to expand, encompassing water treatment,[15,16] gas separation,[17,18] ion separation,[19,20] energy conversion,[21,22] and energy storage.[23–29]

Membrane separation and its associated osmotic phenomena are ubiquitous in nature, playing a crucial role in biological systems.[30,31] Whether in intracellular transport or the selective exchange of ions or compounds, membrane separation mechanisms are vital for sustaining the essential functions and life processes of organisms. For instance, the phospholipid bilayer of cell membranes selectively regulates the transport of angstrom-scale ions (such as K^+, Na^+, Ca^{2+}, Mg^{2+}, and Cl^-)[32] and small molecules (such as water and ATP)[33] in and out of the cell, thus ensuring normal cellular function and metabolic balance.

Biological membranes in nature provide abundant inspiration for the design and synthesis of biomimetic nanoporous membranes, enabling these artificial membranes to achieve ultrahigh ion selectivity and permeability analogous to the biomembranes.[32,33] In comparison, biomimetic nanoporous membranes not only achieve higher ion selectivity and permeability but also exhibit superior chemical, physical, and mechanical stability. Compared with other nanoporous membranes, POF membranes have emerged as the forefront of membrane separation research due to their well-defined pore sizes, expansive surface areas, distinct pore structures, and abundant specific functional groups.[34,35] For example, Cheng et al. created a versatile metal–organic framework (MOF)-based liquid Janus fiber membrane for oil/water separation and heavy metal ion removal. It showed outstanding performance in separating surfactant-stabilized emulsions, with a high flux of 25 310 L m^{-2} h^{-1} bar^{-1}

L. Yang, Z. L. Wang, D. Wei
Chinese Academy of Sciences
Beijing Institute of Nanoenergy and Nanosystems
Beijing 101400, China
E-mail: zhong.wang@mse.gatech.edu
dw344@cam.ac.uk

L. Yang, Z. Wang
School of Chemistry and Life Sciences
Changchun University of Technology
Changchun 130012, China
E-mail: wangzhe@ccut.edu.cn

Z. Wang
Advanced Institute of Materials Science
Changchun University of Technology
Changchun 130012, China

Z. Wang
Key Laboratory of Advanced Functional Polymer Membrane Materials of Jilin Province
Changchun University of Technology
Changchun 130012, China

D. Wei
Centre for Photonic Devices and Sensors
University of Cambridge
9 JJ Thomson Avenue, Cambridge CB3 0FA, UK

and an efficiency exceeding 99.99%.[36] Zhang et al. developed a continuous cationic covalent organic framework (COF)-based membrane by sequentially stacking COF nanosheets (EB-COF:Br) on a porous substrate. This membrane exhibited a water flux exceeding 375 L m^{-2} h^{-1} bar^{-1}. After 30 h of continuous filtration testing, the membrane maintained a steady-state water flux of 48 L m^{-2} h^{-1} bar^{-1}, which is still 20 times higher than that of GO membranes.[37] These characteristics contribute to a better balance between ion selectivity and permeability, exhibiting exceptional osmotic performance and broad application potential.

At present, various nanoporous organic framework membrane materials have been developed, such as MOFs,[38,39] COFs,[40,41] and hydrogen-bonded organic frameworks (HOFs)[42,43] (**Figure 1**). These membrane materials exhibit extensive structural diversity, presenting promising solutions for achieving efficient ion selectivity and ion permeability. Their impressive osmotic performance can be attributed to several

Lixue Yang achieved the M.S. degree from the Henan Normal University in 2023. She continues pursing Ph.D. degree in Changchun University of Technology and is jointly trained by the Beijing Institute of Nanoenergy and Nanosystems, Chinese Academy of Sciences. Her research focuses on the transformation of ions and electrons, with applications in osmotic energy harvesting.

Zhe Wang is a doctoral supervisor at Changchun University of Technology, currently serving as the dean of the College of Chemistry and Life Sciences. His research focuses on the molecular design, structure, morphology, and transport mechanisms of polymer membrane materials. During his research career, he has published over 100 SCI-indexed papers in important academic journals, which have been cited more than 1000 times. He has received two provincial and ministerial second-class awards as the first principal investigator and holds 16 authorized national invention patents. He has led three National Natural Science Foundation general projects, the Ministry of Education's New Century Talent Program, the "Changbai Mountain Scholar" distinguished professor reward program, and over 20 other provincial and ministerial projects, including those funded by Jilin Province's talent development fund, leading talent and project teams, major projects from the Jilin Provincial Department of Science and Technology, the Jilin Provincial Natural Science Foundation, and the Jilin Provincial Development and Reform Commission. Details can be found at: https://www.x-mol.com/groups/wang_zhe.

Zhong Lin Wang received his Ph.D. from Arizona State University in physics. Currently, he is the Hightower Chair in Materials Science and Engineering, Regents' Professor, Engineering Distinguished Professor and Director, Center for Nanostructure Characterization, at Georgia Tech. Dr. Wang has made original and innovative contributions to the synthesis, discovery, characterization and understanding of fundamental physical properties of oxide nanobelts and nanowires, as well as applications of nanowires in energy sciences, electronics, optoelectronics and biological science. His discovery and breakthroughs in developing nanogenerators established the principle and technological road map for harvesting mechanical energy from environment and biological systems for powering personal electronics. His research on self-powered nanosystems has inspired the worldwide effort in academia and industry for studying energy for micro–nano systems, which is now a distinct disciplinary in energy research and future sensor networks. He coined and pioneered the field of piezotronics and piezophototronics by introducing piezoelectric potential gated charge transport process in fabricating new electronic and optoelectronic devices. Details can be found at: http://www.nanoscience.gatech.edu.

Di Wei serves as the principal investigator at BINN and heads the Iontronics Laboratory. As Fellow of the Royal Society of Chemistry (FRSC) and senior member of Wolfson College at Cambridge University, he has published over 100 papers including Nature Energy, Nature Commun., PNAS, Adv Mater, Energ Environ Sci., Matter, etc. as the first/corresponding author. Prof. Wei also has a portfolio of over 200 international patents (including PCT). Notably, 92 patents have been successfully granted, many of which have been transferred to leading companies like Nokia in Finland and Lyten in the USA. Additionally, Prof. Wei has edited three English books, published by Wiley and Cambridge University Press, etc., focusing on nanotechnology for energy and information technology. His achievements have been recognized by the first prize of the Nokia Global Innovation and Excellence Award, Brian Conway Prize in Physical Electrochemistry from the International Society of Electrochemistry (ISE) and various other prizes from ISE and RSC. Details can be found at: http://iontronics.group/en/.

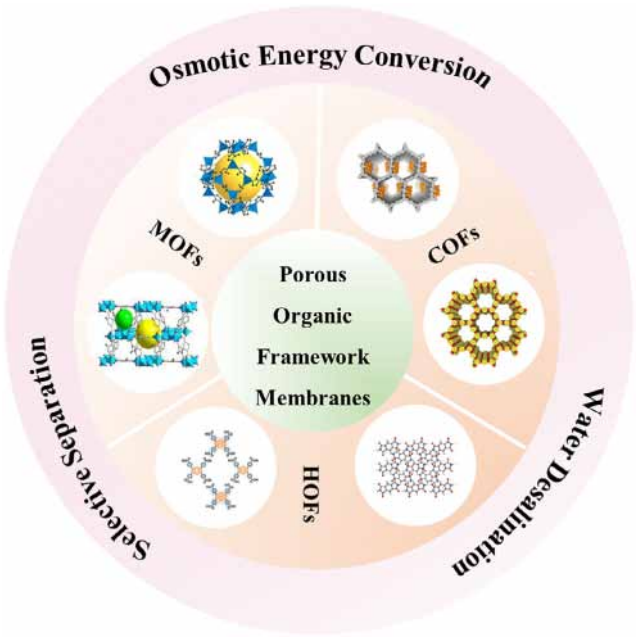

Figure 1. Porous organic framework membranes (MOFs: Reproduced with permission.[38] Copyright 2020, Nature; Reproduced with permission.[39] Copyright 2023, Elsevier), COFs (Reproduced with permission.[40] Copyright 2018, Wiley; Reproduced with permission.[41] Copyright 2019, American Chemical Society), HOFs (Reproduced with permission.[42] Copyright 2021, Wiley; Reproduced with permission.[43] Wiley, Copyright 2024) for osmotic power conversion, seawater desalination, and selective separation.

key factors: 1) precise pore size control, which allows for the effective sieving of ions with different sizes and achieving selective ion transport; 2) surface modification, functional group incorporation, or ligand structure alteration to facilitate chemical functionalization, enhancing the interaction between the membrane material and target ions, further improving ion selectivity; and 3) high porosity and large specific surface area, which provide abundant adsorption sites for ions, significantly increasing ion flux and ensuring high permeability while maintaining high selectivity.

Additionally, the emergence of 2D materials, such as MXene and graphene, has introduced new possibilities for membrane separation technologies.[19,44] These materials offer advantages including high mechanical strength, excellent electrical conductivity, and tunable surface properties, making them attractive for applications in ion sieving and water purification. However, compared to POF membranes, 2D materials still face several challenges, such as insufficient control over pore size, limiting their ability to achieve precise ion selectivity; restricted chemical tunability due to limited functional group diversity; and structural instability under harsh conditions, which affects long-term performance.[45] In contrast, POF membranes, with their well-defined pore architectures and high chemical versatility, provide a more stable and selective platform for ion separation.

Despite the vast potential of POF membranes in osmotic applications, several challenges remain in practical applications. For example, the stability of POF membranes may be compromised in complex environments (such as high temperatures, strong acids, or strong bases), leading to structural degradation or decreased osmotic performance. Additionally, synthesizing high-quality POF membranes typically requires complex and multistep reactions under stringent conditions, which increases technical difficulty and costs in large-scale production. Therefore, optimizing the fabrication methods of POF membranes is crucial. By improving synthesis processes, not only can the osmotic performance of POF membranes be enhanced, but also lower production costs, thereby facilitating broader industrial adoption and feasibility.

This review systematically presents the latest fabrication methods of nanostructured POF membranes. Additionally, we will focus on the impressive progress in harnessing the unique properties of POF membranes in various fields of application such as osmotic power conversion, water desalination, and ion-selective separation. Finally, we anticipate future research directions for POF membranes and discuss the significant challenges. We wish to spotlight the large application potential of these POF membranes by presenting the milestones that have propelled the research in this field into novel and unexpected realms of material chemistry.

2. Fabrication of POFs

2.1. MOF Membranes

To improve the ion selectivity and ion permeability of POF membranes, the fabrication of ultrathin, defect-free POF membranes is paramount. In recent years, with the rapid advancement of materials science, MOF membranes, as a typical representative of POF membranes, have attracted considerable attention. Various synthesis methods have been developed, including heteroepitaxial growth,[46,47] interfacial polymerization,[48,49] in situ growth,[50,51] vapor deposition,[52,53] and electrochemical deposition (**Table 1**).[54,55] For example, Su et al. developed a method for fabricating ultrathin MOF membranes based on anisotropic growth. By employing modified surfactant-assisted polyvinylpyrrolidone (PVP), the growth of zinc-5,10,15,20-tetrakis (4-carboxyphenyl) porphyrin (ZnTCPP) along the *z*-axis was effectively suppressed, resulting in the formation of 2D nanosheets. Subsequently, a vacuum filtration technique was used to prepare ZnTCPP nanosheets with a thickness of only 3.5 nm. The method marked a significant advancement in controlling membrane thickness and uniformity, demonstrating substantial potential for the fabrication of ultrathin, defect-free MOF membranes (**Figure 2**A).[56] Xiao et al. reported a technique for fabricating a heterogeneous sub-nanometer channel membrane. This method involved coating a functionalized self-assembled MOF monolayer onto a porous anodic aluminum oxide (AAO) substrate. The SAMM (self-assembled MOF monolayer) membrane, with a thickness of ≈160 nm, was formed by the self-assembly of zirconium-terephthalate-2-aminoterephthalate (UiO-66-NH_2) nanoparticles (NPs) modified with poly (methyl methacrylate-*co*-vinyl imidazole) at the water–air interface. In this structure, NH_2 and imidazole groups serve as ion filters, significantly enhancing the selective screening of anions. This design integrates narrow pore channels with surface functionalization via positive charges, optimizing both ion selectivity and ion permeability (Figure 2B).[57]

Table 1. Synthesis methods of POFs and their advantages and disadvantages.

Preparation method	Advantages	Disadvantages	Ref.
Solvothermal	Simple and easy to scale up under mild conditions, producing highly crystalline POFs, low defects	Long procedure, hazardous by-products, lowly selective growth of POFs	[78,98]
Encapsulation	Functional enhancement, structural stability improvement, increased tunability	Encapsulation efficiency and uniformity, framework stability risk, increased synthesis complexity	[79]
In situ growth	Maintain pore integrity, uniform distribution, enhanced stability	Potential framework distortion, complex synthesis process, incomplete growth	[80]
Surfactant-assisted	Dimensional control, improved film uniformity, optimized pore structure	Structural integrity risk, pore blockage risk, difficult removal	[56]
Interfacial polymerization	Formation of well-defined POFs, amenable to scalability, preparing POFs thin films, simultaneous control of crystallization and morphology	Limited monomer compatibility, reproducibility is challenging, complexity in designing and engineering of interfaces, requiring the use of specific solvents or surfactants	[83,84], [86,91], [63,64]
Photografting polymerization	Precise surface modification, enhanced interfacial compatibility, mild synthesis conditions	Controllable polymer layer thickness, light source selection and energy control, potential side reactions	[85]
LBL deposition	Precise layer thickness control, interface optimization and heterostructure construction, mild synthesis conditions	Interlayer adhesion challenges, limited deposition uniformity, high demand for interface optimization	[87]
Cathodic deposition	Fast and controllable growth, enhanced interfacial bonding, environmentally friendly	Limited deposition uniformity, requires conductive substrate, complex film thickness control	[88]
In situ hydrothermal synthesis	High crystallinity and purity, formation of uniform and continuous membranes, applicable to various substrate materials	Harsh reaction conditions, slow growth rate, difficulty in controlling film thickness	[89,90]
Polyelectrolyte-induced biomineralization	Promote uniform nucleation and controlled growth, promote anisotropic growth, enhance structural stability	Dependence on polyelectrolytes, affect pore structure, introduce impurities	[93]
Mixed-dimensional strategy	Enhance the structural stability of the membrane, suppress interlayer stacking, improve chemical stability and durability	Complex synthesis process, high size-matching requirements, difficulties in large-scale preparation	[94]
Combining single-mode microwave heating with tertiary growth	Reduce reaction temperature, accelerate synthesis rate, promote uniform membrane growth	High equipment requirements, increased difficulty in controlling membrane thickness, limited defect controllability	[89]
Schiff-based condensation	High chemical tunability, formation of high surface area and ordered channels, suitable for large-scale synthesis	Crystallinity depends on reaction conditions, difficult to control pore size, stability is limited	[97]
PMA strategy	Controllable membrane thickness and structure, enhanced stability and mechanical strength, improved membrane uniformity and scalability	Dependence on polyelectrolytes, polyelectrolyte residue issues, limited porosity of the membrane	[98]
Solution processing method	Simple and efficient, wide applicability, improves membrane flexibility and stability	Limited mechanical strength of the membrane, solvent selectivity and environmental impact, difficulty in controlling membrane thickness	[99]
Self-assembly process	High selectivity and tunability, multifunctionality of materials, no need for complex equipment	Controllability issues in the assembly process, possible aggregation effects, stability issues	[100]

Additionally, Li et al. devised a cross-linking-induced assembly strategy to effectively regulate the balance between the growth and functionalization of MOF membranes. This strategy employs modulators to inhibit the rapid crystallization of MOFs, generating modulator-stabilized MOF clusters (preMOFs). A mild drying process then gradually removes the modulators, allowing the preMOFs to cross-link and form a continuous membrane. The resulting MOF membrane exhibits remarkable surface smoothness, optical transparency, controllable thickness, and scalability, significantly improving the operability and practicality of MOF membranes across various applications (Figure 2C).[58] Huang et al. employed a heteroepitaxial growth strategy to design and fabricate a nanosheet-assembled frame (NAF) membrane assembled from CuBDC (benzene-1,4-dicarboxylate (BDC)) nanosheets. By precisely controlling the nanoscale thickness of molecular penetration through the NAF membrane (≈25 nm), the performance of the NAF membrane was significantly enhanced. Moreover, compared to individual nanosheets, the NAF membrane exhibited superior mechanical stability. This approach provides an effective means of improving both the functionality and durability of membranes (Figure 2D).[59]

2.2. COF Membranes

As the demand for high-performance membrane materials grows, researchers have increasingly explored alternative framework materials with potentially superior properties. Recently, several successful strategies for fabricating COF membranes with specific functionalities have been reported.[60,61] Similar to the synthesis of MOF membranes, interfacial polymerization has proven effective in producing ultra-thin, defect-free COF membranes.[62] Typically, COF precursors are dissolved in two

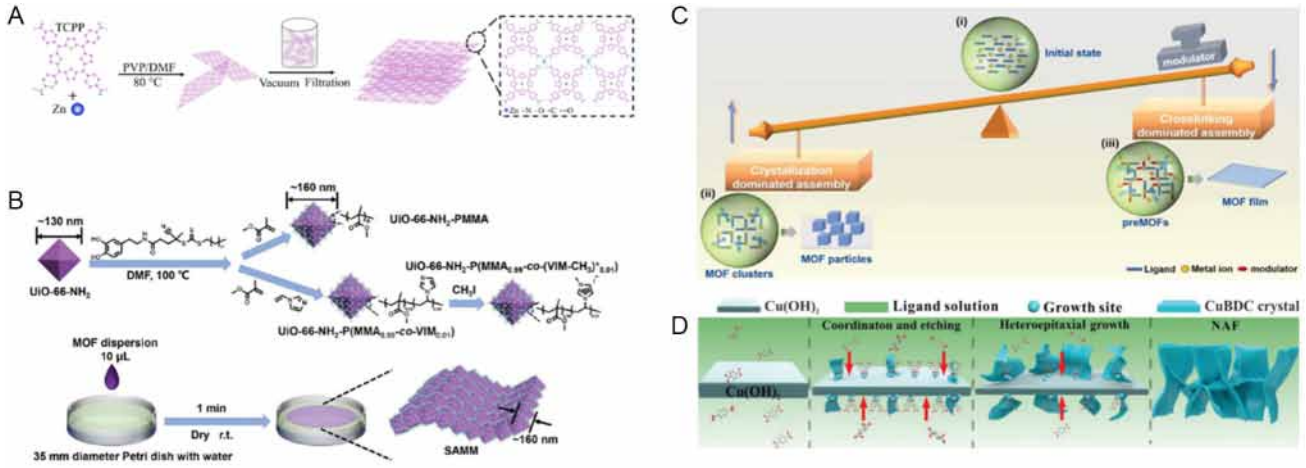

Figure 2. A) Schematic illustration of the preparation process for Zn-TCPP membranes (Reproduced with permission.[56] Copyright 2024, from Royal Society of Chemistry); B) procedure of evaporation-induced interfacial assembly method for SAMM film fabrication (Reproduced with permission.[57] Copyright 2023, Wiley); C) cross-linking-induced assembly strategy for synthesizing MOF membranes (Reproduced with permission.[58] Copyright 2022, Wiley); and D) Schematic representation of the mechanism for the preparation of a CuBDC NAF film (Reproduced with permission.[59] Copyright 2020, Wiley).

immiscible phases, and the reaction occurs at the interface. By controlling reaction conditions and duration, membrane thickness can be fine-tuned. For example, Wang et al. reported an electrochemical interfacial polymerization strategy that actively harnesses self-healing and self-inhibition effects, successfully fabricating an ultrathin COF membrane with a thickness of 85 nm and excellent desalination performance (**Figure 3**A).[63]

Wang et al. pioneered a dual aqueous-phase interfacial assembly method for COF membrane preparation, where polyethylene glycol and dextran aqueous solutions phase-separate into two water-rich phases. Aldehyde and amine monomers are distributed in each phase, forming a COF membrane with a thickness of 5.3 μm at the water–water interface (Figure 3B).[64]

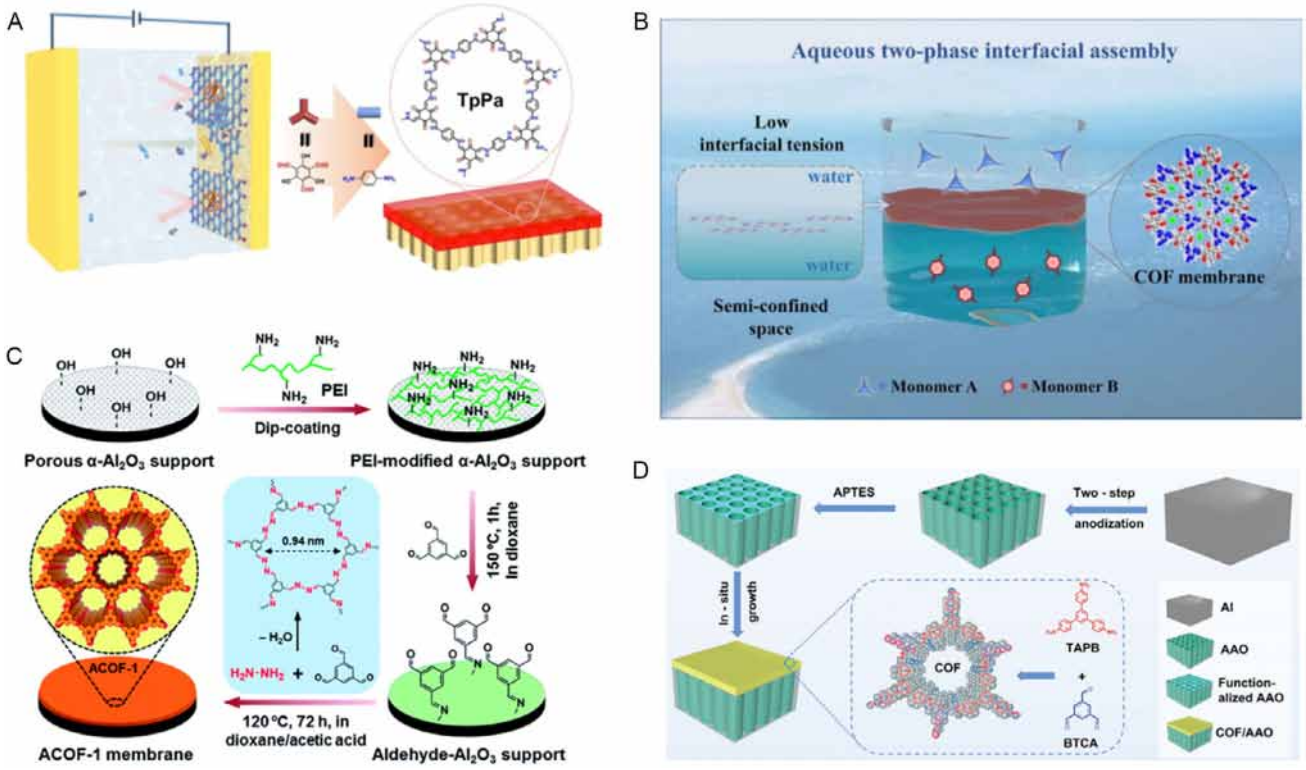

Figure 3. A) Electrochemical interfacial polymerization of an ultrathin TpPa membrane on a PAN substrate (Reproduced with permission.[63] Copyright 2023, Wiley); B) aqueous two-phase interfacial assembly of COF membranes fabrication (Reproduced with permission.[64] Copyright 2022, Nature); C) schematic illustration of the solvothermal synthesis of the ACOF-1 membrane on the porous α-Al_2O_3 support (Reproduced with permission.[65] Copyright 2013, Royal Society of Chemistry); and D) schematic illustration of the fabrication process for the COF/AAO membrane (Reproduced with permission.[66] Copyright 2023, Wiley).

In addition, another strategy for obtaining free-standing, supported pure COF membranes involves growing COF membranes with tailored pore structures on porous substrates. Fan et al. employed a temperature-controlled solvothermal method to continuously adjust the growth of imine-based COF-LZU1 (LZU: Lanzhou University) and ACOF-1 (azine-linked COF), synthesizing a novel bilayer 2D stacked COF–COF composite membrane with an interlaced pore network on a porous substrate (Figure 3C).[65] Chen et al. successfully synthesized an anion-selective membrane with efficient anion transport properties by in situ growing imine-bridged COF on ordered AAO at room temperature (Figure 3D).[66]

The self-assembly method utilizes the spontaneous assembly behavior of COF monomers to form dense COF membranes on the substrate surface. By adjusting the solvent system, concentration, and temperature conditions, the thickness and uniformity of the membrane growth can typically be controlled. Chen et al. prepared a COF–GO composite membrane with ideal nanosheet stacking, tunable thickness, and gas channels by combining 2D COFs with GO through a pH-assisted self-assembly method, achieving a membrane thickness of 1.3 μm (**Figure 4**A).[67] Zhang et al. successfully fabricated COF membranes for salinity gradient energy conversion by employing a layer-by-layer (LBL) electrostatic self-assembly strategy to grow TpDB (1,3,5-triformylphloroglucinol (Tp) and 2,5-diaminobenzoic acid (DB)) COFs in situ on hydrolyzed polyacrylonitrile substrates. The COF membranes contained abundant carboxyl groups, significantly enhancing ion transport selectivity (Figure 4B).[68]

2.3. HOF Membranes

In addition to MOF and COF membranes, supporting membranes composed of other framework materials, such as HOF membranes and POF composite membranes, have also been reported. For example, Wang et al. synthesized a 0.6 μm thick HOF layer in situ on AAO using chemical bonding and solution-processing strategies. The porous structure of this framework, endowed with excellent cation selectivity and ion permeability through hydrogen bonding, π–π interactions, and unprotonated carboxyl groups, enabled the HOF/AAO membrane to exhibit outstanding ion current rectification (ICR) properties. This was attributed to the significant asymmetry of the nanofluidic membrane, resulting from the structure and charge of AAO and HOF, effectively mitigating ion concentration polarization and reducing power loss (**Figure 5**A).[43] Zeng et al. fabricated a 9.12 μm thick metal hydroxide-organic framework membrane with a negatively charged, cation-selective surface on an AAO substrate via a straightforward hydrothermal process. The $Ni_2(OH)_2$@AAO composite membrane significantly enhanced ion flux due to its asymmetric structure and extreme hydrophilicity, effectively facilitating osmotic power harvesting (Figure 5B).[69] Feng et al. successfully fabricated a transparent, fully organic HOF film with excellent reversible electrochromic properties and easy regenerability using an electrophoretic deposition method, which required only 2 min at room temperature (Figure 5C).[70] Zhang et al. proposed a "solution-processing-transformation" strategy, in which methanol vapor was used as a scaffold to sequentially convert a dense amorphous supramolecular coating into a kinetically trapped nonequilibrium HOF-11 film, followed by transformation into a thermodynamically stable crystalline HOF-16 film. The final active and stable HOF-16 film, with a thickness of 0.5 μm, was obtained by removing the methanol scaffold (Figure 5D).[71]

2.4. Hybrid POFs

Given the compositional diversity and structural tunability of MOFs, COFs, and HOFs, POF composite membranes have attracted significant attention in recent years. These composite membranes not only retain advantages such as high crystallinity, well-defined structures, and large specific surface areas, but also offer greater potential for structural and functional modulation. For instance, Liu et al. proposed the concept of an "alloy" membrane (AM) based on the hybridization of MOF and COF, where quaternary ammonium salt (QA)-functionalized COF was incorporated into a polycrystalline zeolitic imidazolate framework-8 (ZIF-8) matrix through electro-driven codeposition. At the interface, the QA-functionalized COF interacted with the ZIF-8 matrix

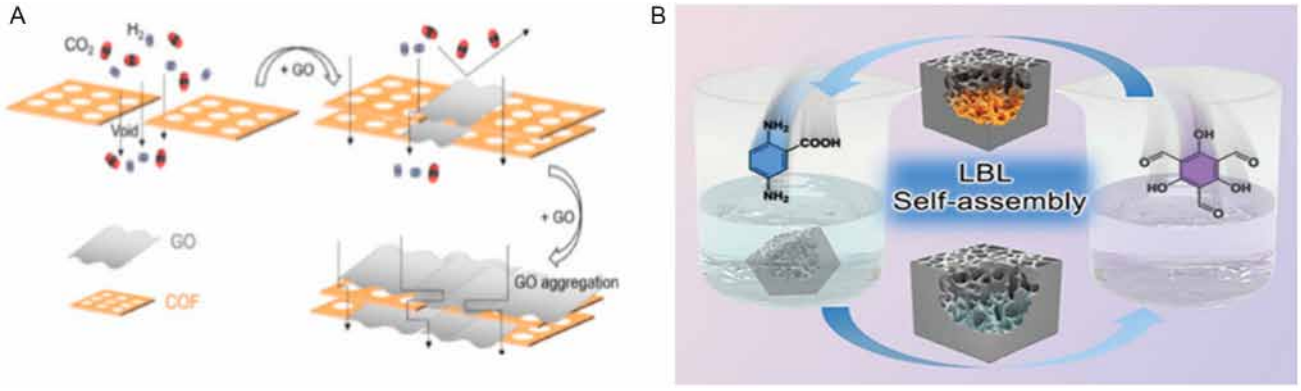

Figure 4. A) Schematic illustration of membrane structures with varying GO loadings for hydrogen separation (Reproduced with permission.[67] Copyright 2024, Elsevier) and B) schematic diagram of COFs membrane synthesis by LBL self-assembly at room temperature (Reproduced with permission.[68] Copyright 2023, Wiley).

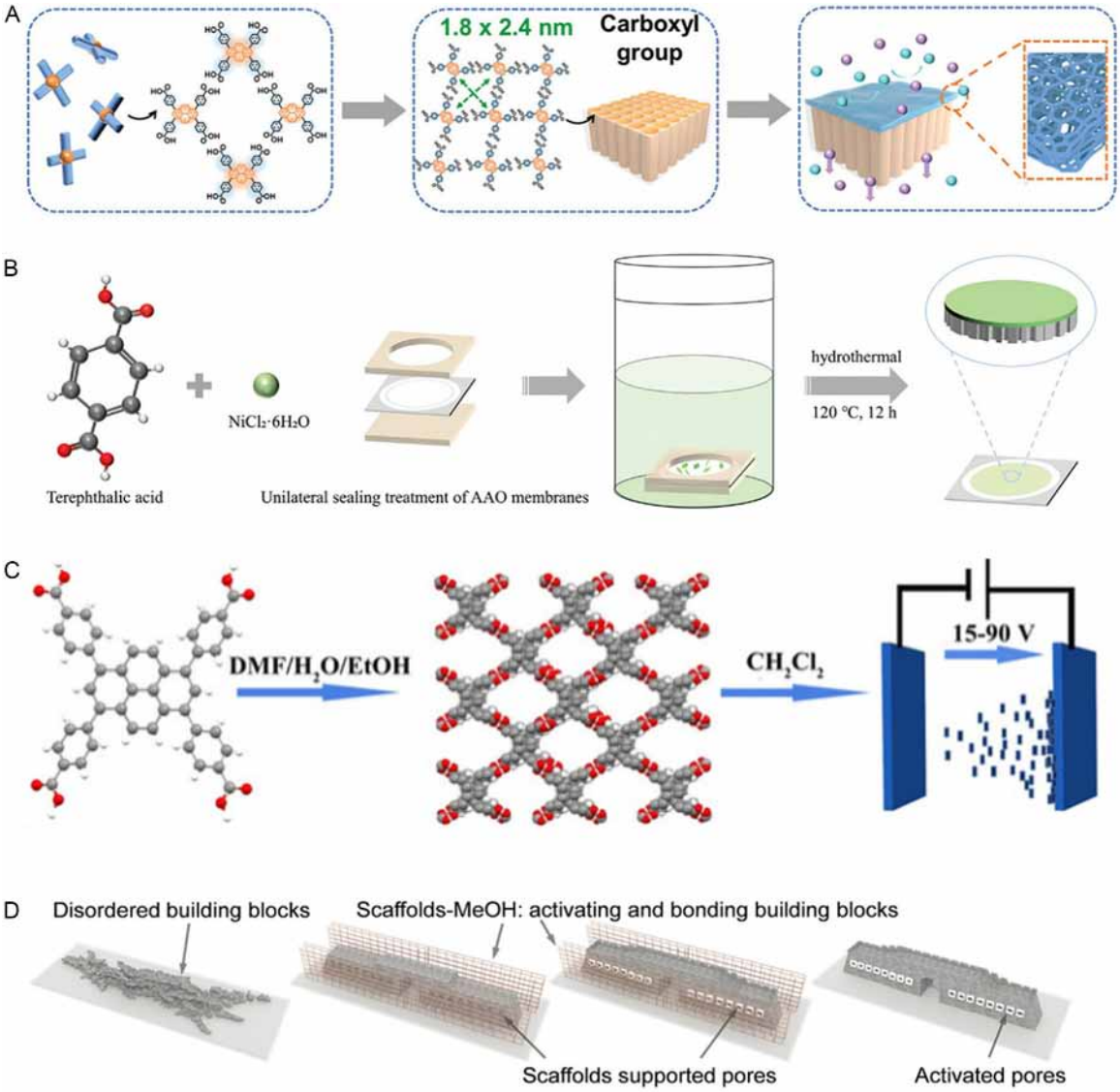

Figure 5. A) Schematic illustration of the HOF membrane fabrication process (Reproduced with permission.[43] Copyright 2024, Wiley); B) diagram illustrating the synthesis of $Ni_2(OH)_2$@AAO composite membranes (Reproduced with permission.[69] Copyright 2024, Wiley); C) fabrication of the nano-PFC-1 film by EPD (Reproduced with permission.[70] Copyright 2020, Wiley); D) schematic diagram of the in situ transformation from an amorphous supramolecular coating to a crystalline HOF membrane with the help of "scaffolds" MeOH, and with TCA monomers as building blocks (Reproduced with permission.[71] Copyright 2024, Wiley).

via Coulombic forces, significantly restricting the rotational freedom of ZIF-8 linkers and triggering a transition from flexible to rigid lattice (the alloy effect). By adjusting the COF loading, AMs with tunable stiffness were achieved (**Figure 6**A).[72] Fu et al. were the first to demonstrate the growth of MOFs on COF membranes, successfully fabricating COF–MOF composite membranes that exhibited higher separation selectivity for H_2/CO_2 gas mixtures compared to individual COF or MOF membranes.[73] Ma et al. used electrospinning and a polymer sacrificial template strategy to prepare a free-standing pure COF (TpPa-1) nanofiber membrane with high crystallinity, good flexibility, excellent mechanical properties, and scalability. Innovatively, this membrane replaced traditional inorganic discs, metal meshes, and polymer membranes as porous supports, and by customizing and confining ZIF-8 growth, COF–MOF composite membranes were prepared on the COF membrane surface and within the COF nanofiber gaps, significantly enhancing the selectivity and permeability for organic dye separation (Figure 6B).[74]

3. Applications of POFs

MOFs, COFs, and HOFs are all nanoporous organic framework materials with distinct structural and chemical properties. MOFs consist of metal nodes connected by organic linkers, offering high tunability in pore size and chemical functionality, making them well suited for applications requiring selective ion transport and stability under diverse conditions.[75] COFs, built entirely from covalently linked organic units, exhibit excellent chemical stability, high porosity, and ordered channels, making them ideal for

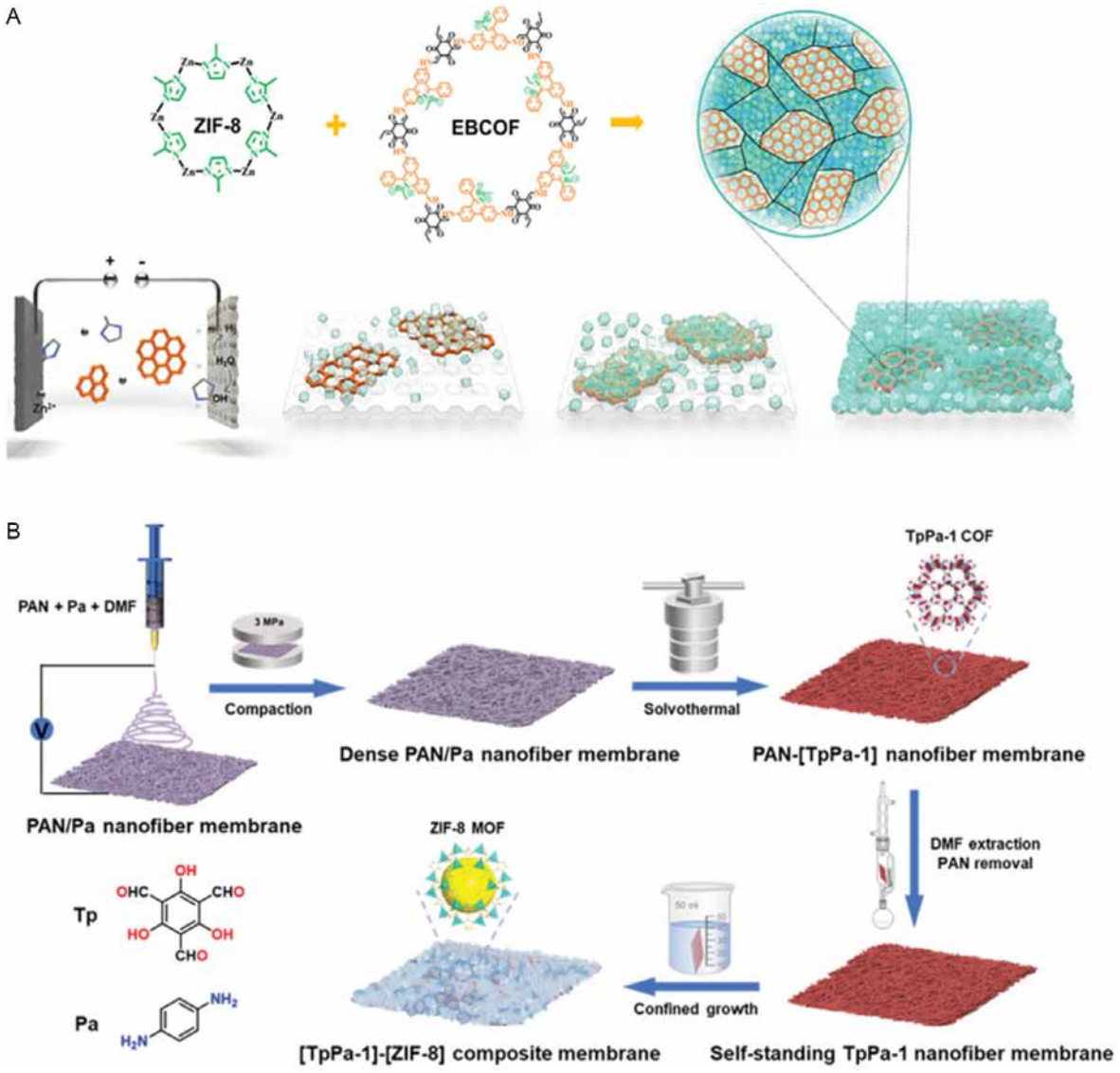

Figure 6. A) Fabrication of MOF–COF AMs through the electro-driven codeposition (Reproduced with permission.[72] Copyright 2022, Wiley) and B) schematic illustration of the preparation process for the [TpPa-1]–[ZIF-8] membrane (Reproduced with permission.[74] Copyright 2024, Wiley).

precise molecular sieving and osmotic energy conversion.[76] In contrast, HOFs rely on reversible hydrogen bonding, enabling solution-processable fabrication and dynamic structural adaptability, which can be advantageous in flexible membrane applications.[77] These inherent differences influence their application in osmotic power conversion, water desalination, and selective separation, as each framework's stability, processability, and transport properties determine its suitability for specific environments.

3.1. Osmotic Power Conversion

Membranes for osmotic power conversion often suffer from the trade-off between the ion selectivity and ion permeability. It is highly desirable to use ion exchange membranes to replace traditional reverse osmosis technology because the membrane-based osmotic power conversion processes are lower energy consumption, higher efficiency, reduced operational costs, and environmentally friendly. Compared to traditional reverse osmosis, ion exchange membranes effectively utilize concentration gradients for efficient energy conversion through selective ion conduction, significantly enhancing selectivity and permeability. Additionally, the pore size and surface characteristics of POF membranes can be precisely adjusted to optimize interactions with solvent molecules, thereby improving permeation flux and conversion efficiency, while the high diversity of nanoporous framework materials ensures stable performance under different solution conditions. Therefore, the ion selectivity and ion permeability of POF membranes are closely related to the intrinsic properties of the materials.

The performance of nanostructured POF membranes in osmotic power conversion is influenced by various factors. For example, the pore structure of the membrane, molecular arrangement, framework flexibility, and interactions with different ions

determine the ion permeation rate and selectivity. In general, many synthesis conditions, such as temperature, solvent, and precursor ratios, can significantly influence the microstructure and final performance of the membranes. By thoroughly exploring these parameters, the osmotic power conversion efficiency of nanostructured POF membranes can be enhanced, leading to more effective energy recovery and resource utilization. Overall, optimizing these factors will provide greater potential for nanostructured POF membranes in osmotic power conversion applications.

3.1.1. MOF Membranes

MOF membrane materials are formed by organic ligands and metal nodes through coordination bonds, providing a unique platform for artificial channel membranes. MOFs exhibit significant advantages in controlling ion selectivity and transport efficiency due to their highly tunable crystal structures and atomically ordered channel structures. By adjusting the pore size and surface functional groups of the MOF membranes, efficient screening of specific ions can be achieved, which is crucial for ion selectivity in osmotic power conversion processes. Wang et al. proposed a biomimetic nanofluidic system based on a 2D copper (II) tetra (4-carboxyphenyl) porphyrin (Cu-TCPP) framework. Its inherent nanoporous structure and horizontal interlayer channels provide a high ionic permeability, with t^+ consistently greater than 0.85 and a power density reaching 16.64 W m^{-2}, surpassing existing nanochannel membranes. Furthermore, thanks to the photothermal properties of Cu-TCPP, light-controlled ion transport can be achieved even under natural light, enhancing ion transport driving forces by combining solar energy and salinity gradients, resulting in an energy conversion performance that achieves a power density of 0.82 W m^{-2} in a symmetric solution system without salinity gradients (**Figure 7**A).[78] Pan et al.

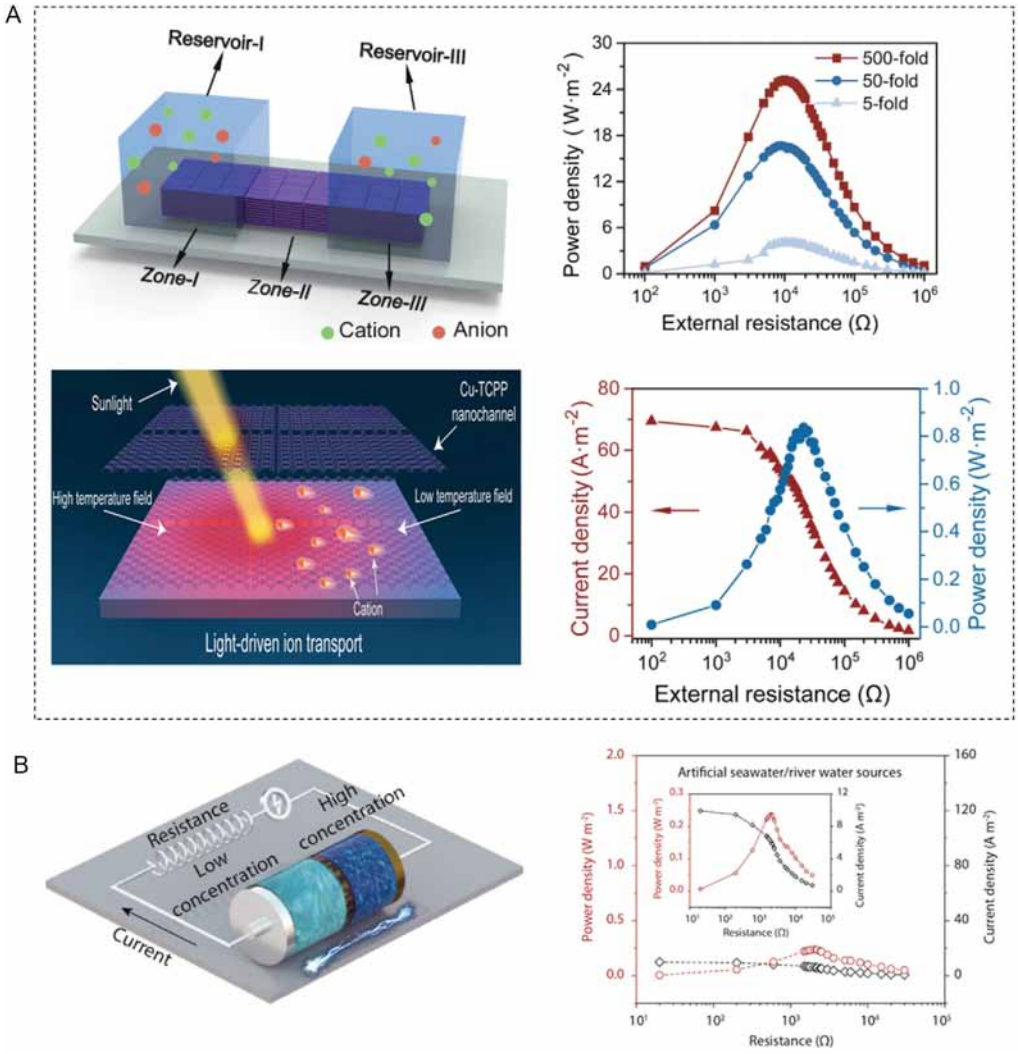

Figure 7. A) Scheme of the ionic energy conversion device; output power density of Cu-TCPP membranes as a function of load resistance under varying salinity gradients; schematic diagram of temperature field generated in Cu-TCPP nanochannels under light irradiation; power density derived from an equilibrium electrolyte solutions system (0.01 M KCl) (Reproduced with permission.[78] Copyright 2024, Nature). B) Schematic representation of the osmotic power density measurement with external resistance; the current density (black diamonds) and output power density (red circles) as a function of external load resistance using artificial seawater and river water were presented (Reproduced with permission.[79] Copyright 2024, Wiley).

encapsulated densely negatively charged poly(sodium-4-styrenesulfonate) within copper-1,3,5-benzenetricarboxylate (HKUST-1)-type porous crystals with a pore size of 0.9 nm, enabling the composite material to generate power through osmosis in high salinity environments while maintaining a negative surface charge for high power density. Experimental showed that when the membrane area was 3×10^{-2} mm^2, t^+ was 0.89, and the power density reached 45.6 W m^{-2}. Even when the membrane area was expanded to about 7 mm^2, the power density remained around 1.7 W m^{-2} (Figure 7B).[79]

Moreover, Liu et al. employed an in situ growth strategy to prepare a light-controllable spirocyclic (SP) encapsulated materials of the institut lavoisier 53 MOF (SP-MIL-53), whose highly ordered sub-nanometer channels can effectively regulate ionic flux through light-driven isomerization, resulting in an intelligent ionic gate with a high switching ratio (16.2). In the open state under a 50-fold KCl concentration gradient, the gate achieved a high power density of 8.3 W m^{-2}. Additionally, density functional theory calculations revealed that the migration constant of K^+ ions in the SP-MIL-53 sub-nanometer channels under UV irradiation (3.61×10^{-2}) is significantly higher than that in the unirradiated state (2.33×10^{-22}) (**Figure 8**A).[80] Su et al. synthesized 2D ZnTCPP nanosheets to construct ion-selective membranes for osmotic power harvesting. The ZnTCPP nanofluidic membrane exhibited sufficient porosity within and between the ZnTCPP nanosheets, achieving a power density of 2.85 W m^{-2}, a cation selectivity of up to 0.9, and an energy conversion efficiency of 30% under a KCl concentration gradient of 0.5 M/0.01 M. When the membrane thickness was reduced to 4 μm, the device's power density increased to 3.01 W m^{-2} (Figure 8B).[56]

Additionally, the nanostructure of the membrane is crucial for osmotic power conversion performance, as its microscopic design directly influences the ion transport directionality and selectivity. Yang et al. proposed a novel nanostructured membrane composed of an ultrathin zirconium-based UiO-66-NH_2 MOF layer and interconnected branched alumina nanotubes, creating a continuous three-layer pore structure ranging from nanometers to submicrons. This significantly enhances ionic directional transport and achieves a high-performance power density of ≈8 W m^{-2} through the synthesis of mixed seawater and river water; under a 50-fold KCl gradient, t^+ reached 0.993, and the power density increased to 17.1 W m^{-2}, with a conversion efficiency of up to 48.5% (**Figure 9**A).[81] Fauziah et al. developed an MOF-based sub-nanopore ionic diode membrane, consisting of a continuous zeolite imidazolate framework-8/poly (styrenesulfonate) membrane and highly ordered alumina nanotube membranes. The asymmetric design optimized the pore size, charge, and wettability, allowing the high negative charge in the MOF layer and the nanometer-scale window pore structure to direct and enhance the transport of Li^+ ions. This resulted in an unprecedented power density of ≈23.4 W m^{-2} when mixing a 2 M LiCl-methanol solution with pure methanol (Figure 9B).[82]

3.1.2. COF Membranes

COFs feature predetermined and atomically ordered channel structures, making them a popular material for manufacturing ion-selective membranes in recent years. The development of COFs offers the potential for large-scale production of membranes that can precisely control channel size, direction, charge

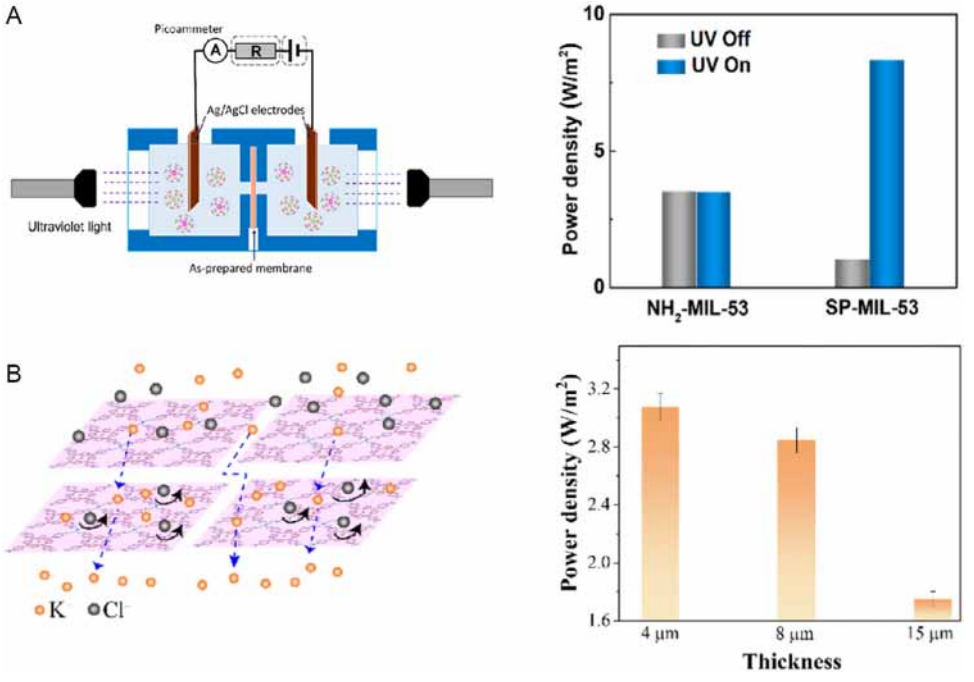

Figure 8. A) Schematic diagram of the experimental setup used for *I–V* measurement and salinity gradient energy conversion; power densities of NH_2-MIL-53 and SP-MIL-53 membranes with UV light off and on (Reproduced with permission.[80] Copyright 2022, American Chemical Society). B) Schematic illustration of ion transport through the membrane in salinity gradients; power density of membranes with different thicknesses under 0.5/0.01 M KCl solution (Reproduced with permission.[56] Royal Society of Chemistry, Copyright 2024).

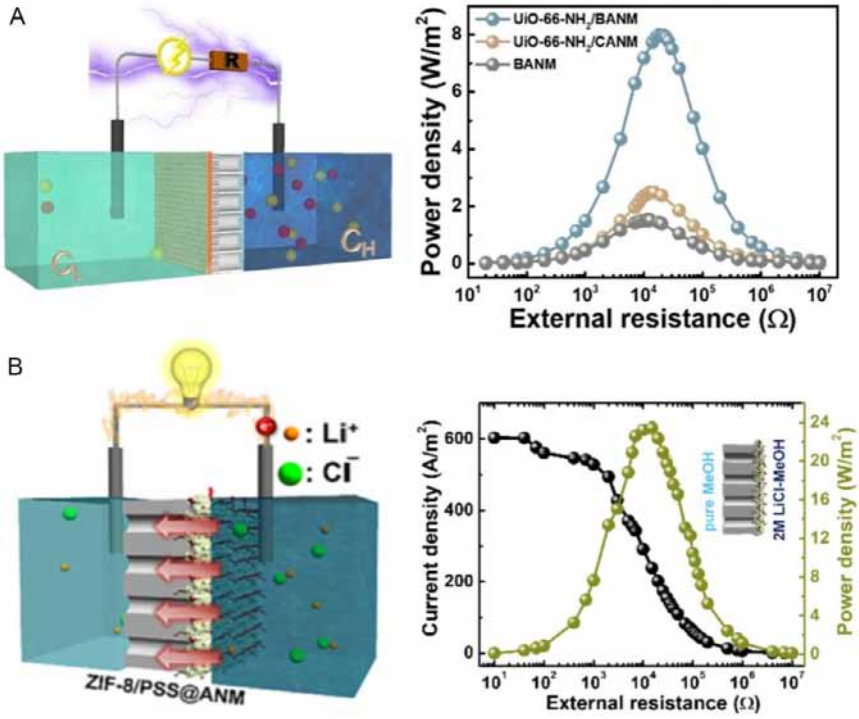

Figure 9. A) Schematic representation of the zirconium-based MOF heterogeneous membrane for harvesting energy in a salinity gradient (Reproduced with permission.[81] Copyright 2024, Wiley); the power density under the condition of mixing the artificial seawater and the river water. B) Schematic illustration of the experimental setup for osmotic power conversion (Reproduced with permission.[82] Copyright 2022, Elsevier).

polarity, and density. Lai et al. developed a COF membrane containing dipolar benzothiazole units, which, due to its robust nanoscopic channels, can modulate the membrane surface charge through ion-dipole interactions, providing customizable ion transport characteristics. After treatment with Na_3PO_4, the membrane's negative charge was enhanced, significantly improving cation selectivity and osmotic power conversion efficiency, achieving an output power density of 155 W m^{-2} under 0.5 and 0.01 M NaCl conditions (**Figure 10**A).[83] Yin et al. manipulated the bonding within a covalent organic framework membrane to

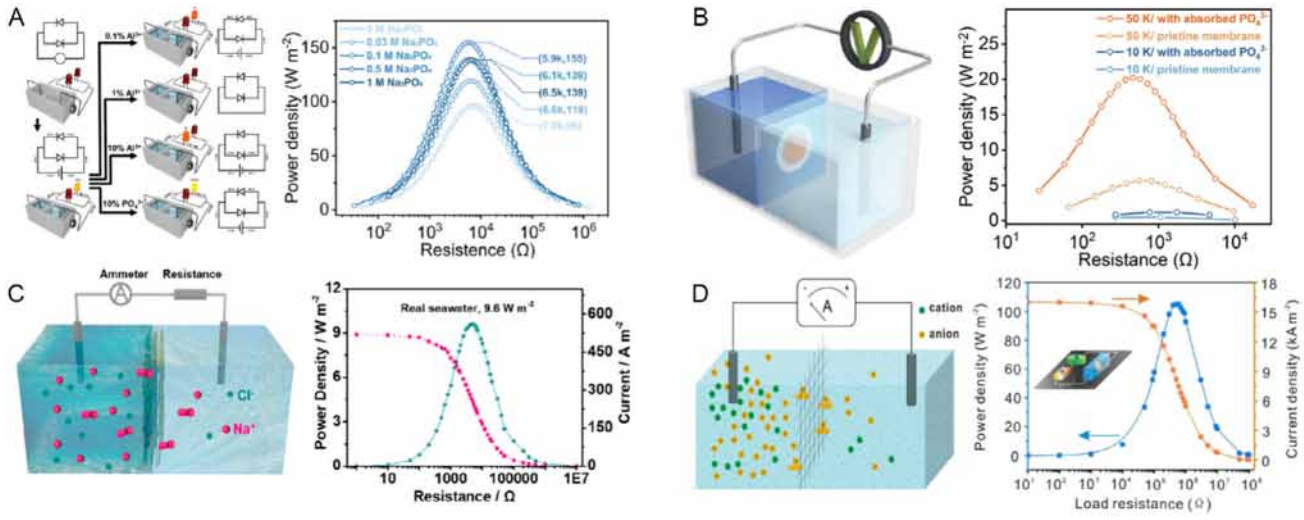

Figure 10. A) Visualization of the variations in output potential and current direction in response to the presence of different additional ions; maximum output power density observed in the presence of 0.5 and 0.01 M NaCl for the COF-TAPB-BDTA membrane treated with various conditions of Na_3PO_4 (Reproduced with permission.[83] Copyright 2024, Wiley); B) schematic of the setup utilized for transmembrane ionic transport experiments; plots showing the electricity delivered to an external circuit with load resistance under a 3 M KCl (Reproduced with permission.[84] Copyright 2024, Nature); C) schematic of the osmotic power conversion process; power density of a PyPa-SO_3H/SANF membrane with natural seawater/river water with a resistance load of 5 KΩ (Reproduced with permission.[85] Copyright 2021, American Chemical Society); and D) illustration of the experimental setup for osmotic power generation; performance of the ZnTPPVg COF membrane in osmotic power generation with 0.5 M/0.01 M NaCl (Reproduced with permission.[86] Copyright 2022, American Chemical Society).

alter the electrostatic potential distribution, successfully achieving cation selectivity in a charge-neutral membrane with β-ketoamine bonds in high-salinity environments while maintaining super-selectivity under temperature gradients, offering a new method for converting low-grade waste heat into electrical energy. Experimental results showed that in a 3 M KCl solution with a 50 K temperature difference, the membrane achieved an output power density of 5.70 W m^{-2}, which increased to 20.22 W m^{-2} after treatment with K_3PO_4, 3.6 times that of the untreated membrane (Figure 10B).[84] Man et al. reported a nanocomposite membrane formed by coupling 2D sulfonated COF nanosheets with anionic-grafted aramid nanofibers (ANFs), featuring a biomimetic membrane structure that enables high-performance osmotic power generation. Theoretical and experimental studies indicate that COF nanosheets provide abundant nanofluid channels, synergistically facilitating ultrafast ionic migration and achieving high cation selectivity through covalently bound anions, while the grafted ANFs enhance the mechanical strength of the membrane and improve ion diffusion/rectification; in osmotic power devices, the biomimetic membrane exhibits a power density of 9.6 W m^{-2} (Figure 10C).[85] Huang et al. demonstrated a molecularly thin 2D COF monolayer membrane with extreme thickness, high porosity, and a tight pore distribution, serving as an efficient osmotic power device. Its pore size can reach 3.8 nm and surface charge density as low as 2.2 mC m^{-2}, yet under a 50-fold NaCl concentration gradient (0.5 M/0.01 M), it achieves a permeation current density of 16.7 kA m^{-2} and an output power density of 102 W m^{-2}, which can be further enhanced to 170 W m^{-2} in practical seawater/river water gradient systems (Figure 10D).[86]

3.1.3. HOF Membranes

HOFs are framework materials formed through intermolecular hydrogen bonding, with these bonds further reinforced by other weak interactions, such as π–π stacking. In the field of osmotic power conversion, HOF materials offer the advantage of being easily regenerated and reused through simple recrystallization, which provides a significant edge over existing porous materials. In contrast, MOFs and COFs exhibit customizable nanochannels and structural advantages in osmotic power conversion, but their synthesis often requires careful selection of appropriate ligands, posing challenges for large-scale production. Notably, due to the reversibility of hydrogen bonding, HOFs can dissolve in organic solvents, allowing them to be fabricated via straightforward solution processing methods, bypassing the need for complex ligand selection. Additionally, HOF membranes retain their crystalline nanoporous structures while offering unique advantages such as low cost, ease of purification, and the ability to be repaired through simple recrystallization. These properties further enhance their potential for applications in osmotic power conversion. For example, by growing HOF in situ on AAO, a HOF/AAO nanofluidic membrane was formed. Owing to the significant asymmetry in structure and charge between AAO and HOF, the HOF/AAO membrane exhibited excellent ICR properties, achieving a power density of 75.2 W m^{-2} under a 500-fold NaCl concentration gradient (**Figure 11**).[43]

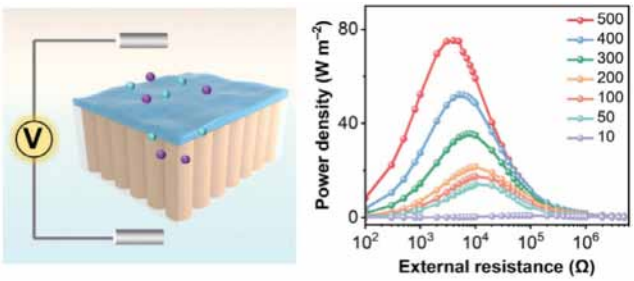

Figure 11. An electrochemical setup was employed for *I–V* measurement; power densities of the HOF/AAO with increasing loaded resistance under a series of NaCl salinity gradients (Reproduced with permission.[43] Copyright 2024, Wiley).

3.1.4. Hybrid POFs

Tonnah et al. fabricated a bilayer hybrid MOF (MOF-on-MOF) membrane by depositing ZIF-8 onto a UiO-66-NH_2 membrane embedded with poly(4-styrenesulfonic acid) (PSS), achieving efficient transmembrane conductivity and enhanced osmotic power generation. The sub-nanometer cavities in the ZIF-8 layer promote ionic selectivity through size exclusion, while the PSS-embedded UiO-66-NH_2 membrane ensures cation permeability. Under a salinity gradient of 3 kΩ and 9.20 W m^{-2}, the overlapping double electric layer generates a permeability of 40.01 W m^{-2} and 665 A m^{-2}, enhancing ionic transport and selectivity (**Figure 12**A).[87] Li et al. synthesized a Janus MOF (J-MOF) membrane composed of ZIF-8 and UiO-66-$(COOH)_2$ using electrodeposition techniques, which exhibits rapid ionic transport and exceptional ionic selectivity. The asymmetric structure and surface charge distribution effectively suppress ionic concentration polarization, enhancing charge separation, and ultimately achieving an output power density of 3.44 W m^{-2} under a 1000-fold salinity gradient (Figure 12B).[88]

3.2. Water Desalination

Desalination of saline water has the potential to effectively address the water scarcity. The desalination method based on POF membranes utilizes their tunable pore structure and excellent selectivity to achieve efficient separation of water molecules from salt ions. This membrane design not only ensures a high water permeability but also significantly reduces salt permeability, thereby enhancing desalination efficiency. Furthermore, the lightweight and renewable characteristics of POF membranes provide substantial economic potential in practical applications.

Cong et al. prepared a continuous aluminum MOF-303 membrane on an α-Al_2O_3 substrate using an in situ hydrothermal method. Leveraging sieving and electrostatic repulsion mechanisms, this membrane exhibits an excellent permeability of 3.0 L m^{-2} h^{-1} bar^{-1} μm and a high rejection rate for divalent ions (e.g., 93.5% for $MgCl_2$ and 96.0% for Na_2SO_4). Its water permeability exceeds that of conventional zirconium MOFs, zeolites, and commercial polymer reverse osmosis and nanofiltration (NF) membranes, while the membrane material demonstrates good stability and low production costs (**Figure 13**A).[89] Liu et al. synthesized a pure-phase Zr-MOF (UiO-66) polycrystalline membrane

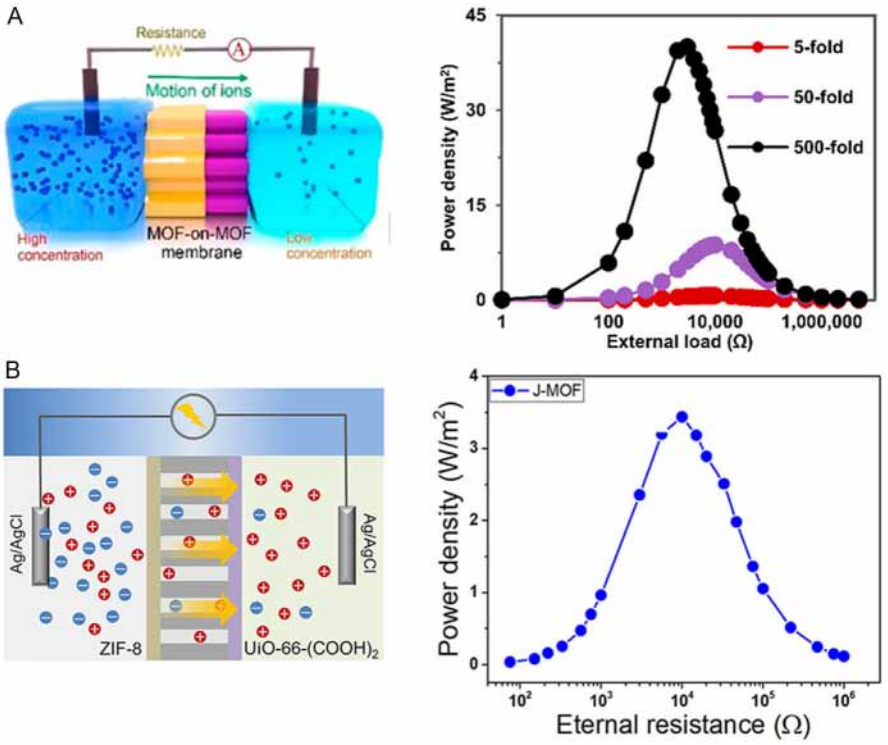

Figure 12. A) Schematic illustration of the osmotic power generation setup with the supplying external load resistances; power densities for NaCl under external resistance corresponding to fivefold, 50-fold, and 500-fold salinity gradients, respectively (Reproduced with permission.[87] Copyright 2023, American Chemical Society). B) Schematic illustration of ion charge separation on the J-MOF membrane; output power densities of the J-MOF membrane connected to varying external resistances (Reproduced with permission.[88] Copyright 2023, American Chemical Society).

on alumina hollow fibers using an in situ solvothermal synthesis method. Single gas permeation and ion rejection tests confirmed the membrane's integrity and functionality, showing moderate permeability (0.14 L m^{-2} h^{-1} bar^{-1} μm) and good permeability (0.28 L m^{-2} h^{-1} bar^{-1} μm), along with exceptional multivalent ion rejection performance (e.g., 86.3% for Ca^{2+}, 98.0% for Mg^{2+}, and 99.3% for Al^{3+}). Moreover, no performance degradation was observed during various saltwater solution tests lasting up to 170 h, benefiting from the chemical stability of the UiO-66 material (Figure 13B).[90] You et al. functionalized the surface of ZIF-8 NPs using polyethyleneimine (PEI) and employed trimesoyl chloride as a cross-linker to integrate them into the selective layer through confined interfacial polymerization, successfully fabricating a ZIF-8-based nanocomposite membrane. With a ZIF-8 NP content of up to 70 wt%, this membrane provided numerous transport channels, significantly enhancing seawater desalination permeability (>43.6 LMH bar^{-1}). Additionally, the polyamide formed during interfacial polymerization filled the gaps between ZIF-8 NPs, ensuring a high Na_2SO_4 rejection rate (≈95.1%) (Figure 13C).[91] Wang et al. developed an antifouling MOF membrane by growing metal azolate framework-4 (MAF-4) in situ on a polyethersulfone (PES) substrate as a base layer, followed by epitaxial growth of a crystalline metal azolate framework-7 (MAF-7) outer shell. The base layer, via chelation, enhanced desalination performance, while the MAF-7 outer shell, with unbound nitrogen atoms, imparted hydrophilicity and smoothness, promoting permeability and fouling resistance. As a result, the MAF-7@4/PES membrane achieved a NaCl rejection rate of 98.7%, a permeability of 1.24 L m^{-2} h^{-1} MPa^{-1}, and a flux decline rate of 22.4% when tested using bovine serum albumin (BSA) as a model foulant.[92]

In addition to MOF membranes, COF membranes, characterized by high porosity, ordered channel structures, and chemical stability, present new avenues for addressing seawater desalination challenges. Inspired by biomineralization processes, Zhao et al. synthesized covalent organic framework nanosheets (CON) using branched PEI and dioxin-linked COF with excellent planarity, providing nucleation sites for the preassembly of COF monomers, inhibiting π–π interactions through protonation, and promoting anisotropic growth, resulting in membranes with a permeability of 341 kg m^{-2} h^{-1} and a desalination rate of 99.5% (**Figure 14**A).[93] Wang et al. introduced a technique for fabricating COF membranes through a double-water-phase interfacial assembly method, using aqueous solutions containing polyethylene glycol and dextran to separate into two aqueous-rich phases, in which aldehyde and amine monomers were distributed, leading to a series of COF membranes with NaCl rejection rates of 93.0–93.6% and permeabilities of 1.7–3.7 L m^{-2} h^{-1} bar^{-1} (Figure 14B).[64] Furthermore, Wang et al. connected TpPa-SO_3H (Pa-SO_3H: diaminobenzene sulfonic acid) nanosheets with TpTTPA (TTPA: 5,5′,5″-(1,3,5-triazine-2,4,6-triyl) tris (pyridin-2-amine) nanoribbons through electrostatic and π–π interactions, constructing an ordered and robust structure with COF membranes that achieved ultrafast desalination. The optimized membranes demonstrated a NaCl removal rate of 99.91% and a water flux of 267 kg m^{-2} h^{-1}, along with excellent antifouling properties, supporting superior operational stability

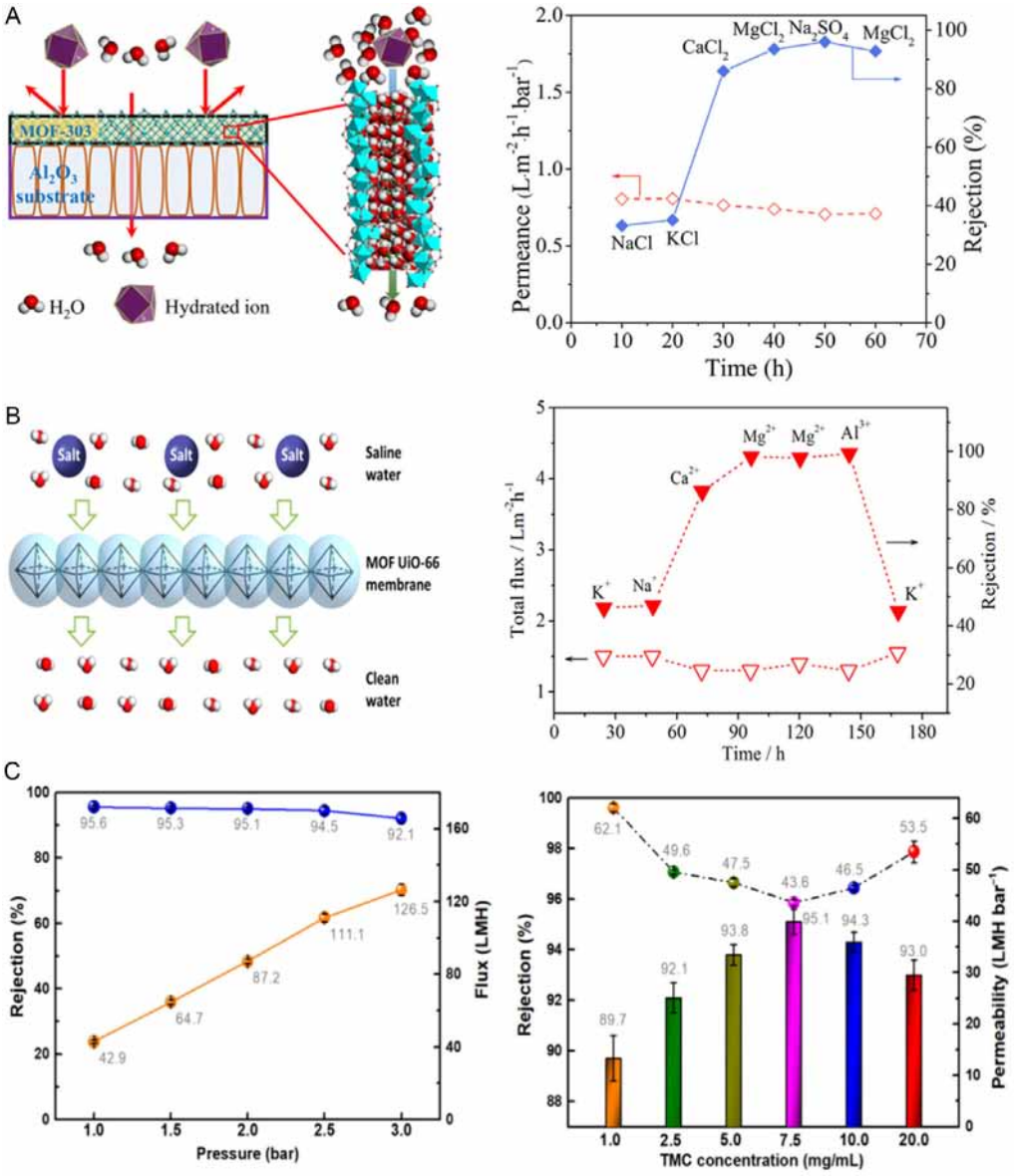

Figure 13. A) Schematic representation of water desalination using a MOF-303 membrane; separation performance of the MOF-303 membrane for water desalination (Reproduced with permission.[89] Copyright 2021, American Chemical Society); B) desalination performance of the UiO-66 membrane (Reproduced with permission.[90] Copyright 2015, American Chemical Society); and C) effect of the TMC concentration on Na_2SO_4 separation performance; separation performance of the nanocomposite membrane at 7.5 mg mL^{-1} TMC as a function of applied pressure (Reproduced with permission.[91] Copyright 2024, Elsevier).

(108 h) and high salinity tolerance (7.5 wt%), indicating significant practical application potential (Figure 14C).[94] Wang et al. reported an electrochemical interfacial polymerization strategy that successfully produced ultrathin COF membranes with a thickness of 85 nm by actively regulating self-healing and self-inhibition effects. These membranes showcased outstanding seawater desalination performance, achieving a permeation flux of 92 kg m^{-2} h^{-1} and a removal rate of up to 99.96% (Figure 14D).[63]

3.3. Selective Separation

3.3.1. Gas Separation

POF membranes exhibit great potential in the field of selective separation, particularly in gas separation. The unique structural characteristics of POF membranes, including high porosity, tunable pore size, and good chemical stability, enable them to selectively separate specific molecules. Precise pore size tuning is crucial for optimizing separation performance. For example, functional group modification and the choice of synthesis solvent can alter interlayer interactions, thereby adjusting the pore size and ultimately influencing the pore structure. These factors collectively determine the membrane's selectivity and permeability.[95] Compared to traditional membrane materials, POF membranes not only enhance separation efficiency but also maintain excellent stability under operational conditions, making them suitable for various complex separation environments.

For example, Kong et al. proposed a universal strategy for designing and preparing novel MOF-based hybrid membranes. The resulting MOF/organic silica nanocomposite membranes

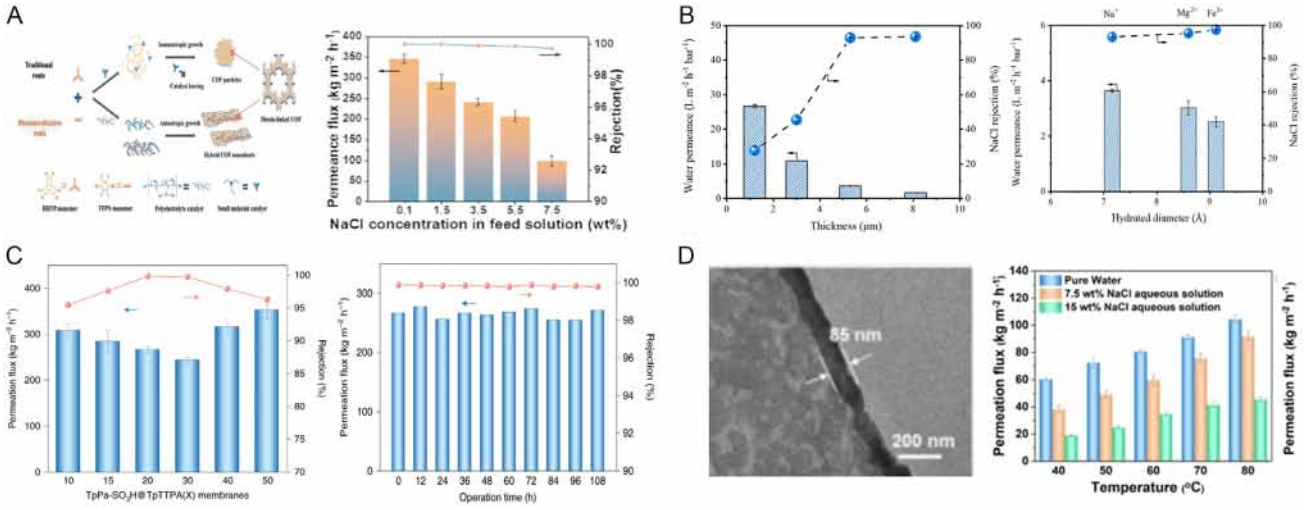

Figure 14. A) Mineralization-inspired synthesis of ultrahigh aspect ratio hybrid COF nanosheets; desalination performance of the PEI-10000-COF@(20)CNC membrane in various salinity solutions (Reproduced with permission.[93] Copyright 2024, Wiley); B) performance of membranes with different thickness and those subjected to different salinity solutions (Reproduced with permission.[64] Copyright 2022, Nature); C) desalination performance of TpPa-SO_3H@TpTTPA(*X*) membranes; long-term operational stability of the TpPa-SO_3H@TpTTPA(20) membrane (Reproduced with permission.[94] Copyright 2022, Nature); D) cross-sectional TEM images of TpPa membranes obtained at different electrochemical time; temperature-dependent permeation flux of the TpPa@PAN-4.0 membrane in different salinity (Reproduced with permission.[63] Copyright 2023, Wiley).

are tightly bonded to tubular ceramic substrates and exhibit excellent gas separation performance. In particular, the pore structures of ZIF-8 and MIL-53-NH_2 significantly influence separation efficiency, as their intrinsic pore sizes and surface chemistry dictate gas diffusion and adsorption behaviors. The membranes doped with ZIF-8 and MIL-53-NH_2 show the best selectivity and permeability for H_2/CH_4 and CO_2/CH_4 mixtures at room temperature, with H_2/CH_4 selectivity of 26.5 and permeability of 1.06×10^{-6} mol m^{-2} s^{-1} Pa^{-1}, and CO_2/CH_4 selectivity of 18.2 and permeability of 1.44×10^{-7} mol m^{-2} s^{-1} Pa^{-1} (**Figure 15**A).[96] Wang et al. utilized the $Ti_8(\mu_2\text{-}O)_8(OOCC_6H_5)_{16}$ cluster as the titanium source for the MIL-125 membrane, resulting in a lower reaction temperature and a higher number of framework defects, thereby enhancing CO_2/N_2 adsorption selectivity. The introduction of framework defects effectively modifies the pore environment, which influences the adsorption and transport properties of gas molecules. The ideal CO_2/N_2 selectivity of the MIL-125 membrane, prepared by combining single-mode microwave heating with a three-stage growth method, reached 38.7, ranking highest among original MOF membranes under the same conditions. Additionally, the ideal selectivities for H_2/N_2 and H_2/CH_4 reached 64.9 and 40.7, respectively, indicating broad application potential in gas separation (Figure 15B).[97]

Recently, Fan et al. synthesized a diazine-linked ACOF-1 membrane on a PEI-modified porous α-Al_2O_3 substrate via a solvothermal method, where PEI improved surface uniformity by filling macropore defects through hydrogen bonding, enhancing support integrity and providing NH_2 groups for grafting, thereby indirectly influencing the membrane's porosity and achieving a CO_2/CH_4 selectivity of 86.3 with a CO_2 permeability of 9.9×10^{-9} mol m^{-2} s^{-1} Pa^{-1} (**Figure 16**A).[98] Li et al. proposed a novel synthesis strategy, successfully fabricating continuous and complete self-standing COF membranes, including 2D N-COF membranes and 3D COF-300 membranes. Both membranes demonstrated excellent H_2 selectivity in H_2/CO_2 gas separation, with N-COF showing a selectivity of 13.8 and COF-300 showing a selectivity of 11, while exhibiting ultrahigh H_2 permeability of 4319 GPU for N-COF and 5160 GPU for COF-300 (Figure 16B).[99]

Li et al. designed and synthesized functional COF membranes using 1,3,5-triformylbenzene (TP) and isoquinoline-5,8-diamine (IQD) as monomers. The TP-IQD framework features a pore size of 6.5 Å and a surface area of 289 m^2 g^{-1}. Nanoflakes ≈4 nm thick were prepared via mechanical exfoliation and were incorporated with the 6FDA-ODA (6-fluoro-2,3,5,6-tetrafluorobenzene-1,4-diamine) polymer to create mixed matrix membranes. The precise control of pore size and interfacial compatibility between the COF nanoflakes and polymer matrix significantly enhanced the permeability of C_2H_2 and the selectivity of C_2H_2/C_2H_4, achieving increases of 160% and 430%, respectively, compared to pure 6FDA-ODA (Figure 16C).[100] Wang et al. developed a poly-electrolyte-mediated assembly (PMA) strategy to fabricate ultrathin ionic COF membranes with a thickness of up to 8 nm, achieving efficient CO_2 separation, with the membranes exhibiting a CO_2 permeability of 1371 GPU and a CO_2/N_2 selectivity of 33 for simulated flue gas (Figure 16D).[101] The introduction of ionic functionalities within the COF framework not only regulated the pore environment but also enhanced gas–membrane interactions, demonstrating the impact of functional modifications on separation efficiency.

HOFs exhibit excellent selectivity and permeability due to their hydrogen bonding characteristics, along with structural flexibility, high thermal stability, and regeneration capability, making them ideal materials for efficient gas separation. Feng et al. constructed a stable and flexible porous hydrogen-bonded organic framework (UPC-HOF-6) and successfully prepared membranes of this framework by optimizing precipitation conditions, demonstrating outstanding selectivity and pressure responsiveness in H_2/N_2 separation. This performance benefits from abundant

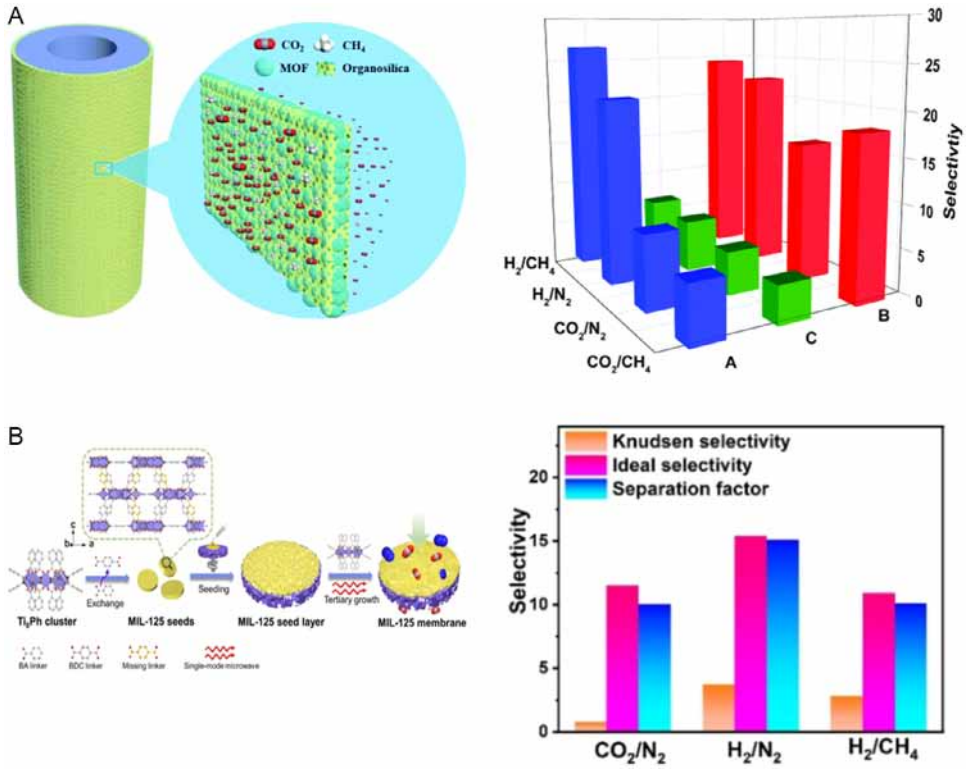

Figure 15. A) Schematic illustration of a MOF/organosilica nanocomposite membrane supported on a tubular alumina substrate for gas separation; the selectivities of H_2/CH_4, H_2/N_2, CO_2/CH_4, and CO_2/N_2 mixture gases through the ZIF-8/organosilica, MIL-53-NH_2/organosilica, and CAU-1-NH_2/organosilica membranes (Reproduced with permission.[96] Copyright 2017, Royal Society of Chemistry). B) Schematic illustration of the preparation of a defective MIL-125 membrane with a Ti_8Ph cluster source by combing single-mode microwave heating with tertiary growth; the separation factor for CO_2/N_2, H_2/N_2, and H_2/CH_4 gas pairs on the MIL-125-SG membrane (Reproduced with permission.[97] Copyright 2022, Wiley).

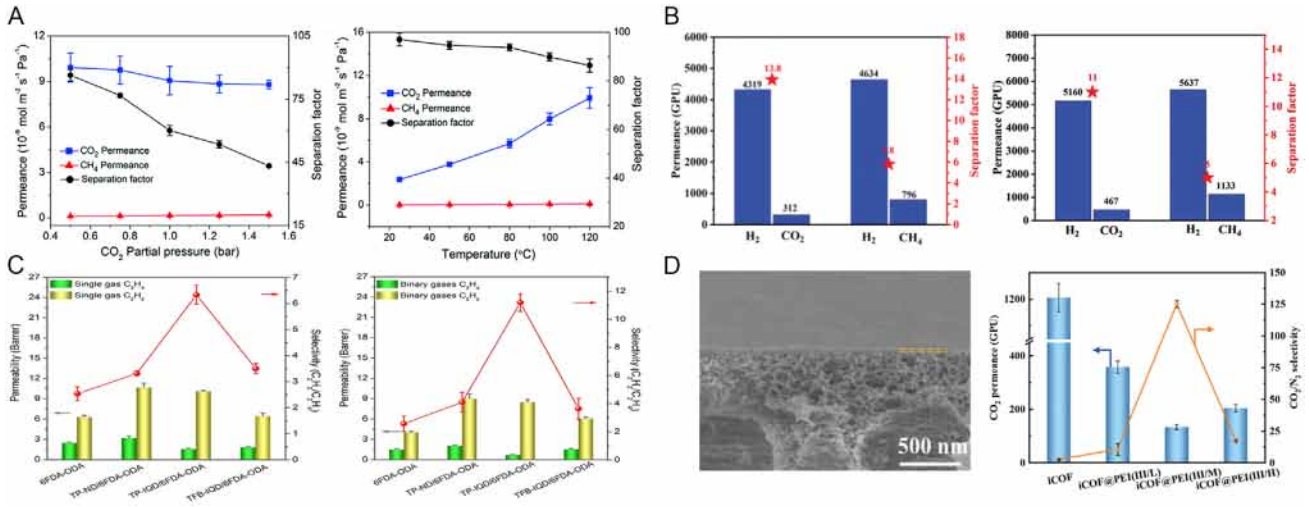

Figure 16. A) CO_2 permeance and CO_2/CH_4 separation factor of the ACOF-1 membrane as functions of the (a) CO_2 partial pressure at 120 °C and (b) permeation temperature at 1 bar (Reproduced with permission.[98] Copyright 2018, Royal Society of Chemistry); B) the separation performance of equimolar binary gas mixtures for the N-COF membrane and the COF-300 membrane (Reproduced with permission.[99] Copyright 2023, Wiley); C) the single and binary C_2H_2/C_2H_4 separation performances of the 6FDA-ODA, TP-ND/6FDA-ODA, TP-IQD/6FDA-ODA, and TFB-IQD/6FDA-ODA membranes (Reproduced with permission.[100] Copyright 2023, Wiley); and D) cross-sectional SEM image of the iCOF@PEI(III/M) membrane; separation performances of the pristine iCOF and iCOF@PEI(III/Y) membranes (Reproduced with permission.[101] Copyright 2023, Wiley).

hydrogen bonds, strong π–π interactions, and the self-healing capability of the membranes (**Figure 17**A).[102] Wang et al. showcased the application of HOF-based mixed matrix membranes in carbon dioxide separation, using the unique MOF HOF-21 as a filler, which is uniformly dispersed within Pebax polymer. HOF-21 features a moderate pore size (0.35 nm) and excellent moisture stability; its multiple binding sites and continuous hydrogen bonding network facilitate efficient CO_2 transport. The resulting

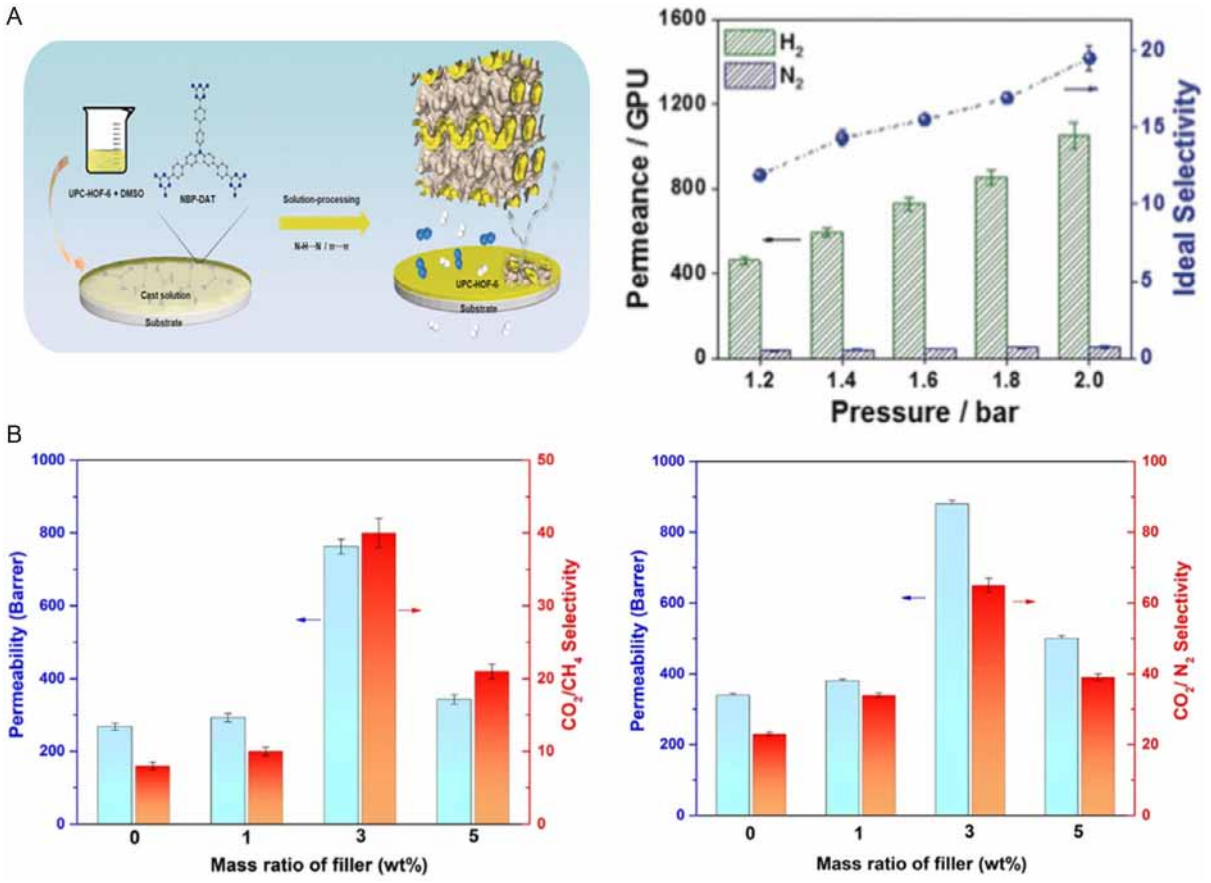

Figure 17. A) HOF membrane has been fabricated by simple solution-processing techniques; the single gas permeation characteristics of the UPC-HOF-6-120 membrane at 25 °C (Reproduced with permission.[102] Copyright 2020, Wiley). B) Separation performance of CO_2/CH_4 and CO_2/N_2 mixed gas separation performance of MMMs with different filler loadings (Reproduced with permission.[103] Copyright 2023, Nature).

membranes achieved a permeability exceeding 750 bar, with selectivity for CO_2/CH_4 and CO_2/N_2 of ≈40 and 60, respectively (Figure 17B).[103]

3.3.2. Chiral Separation

Chiral separation is a key technique for the separation and purification of enantiomers, playing a crucial role in pharmaceuticals, agrochemicals, food additives, and fine chemicals.[104,105] Since enantiomers can exhibit significantly different physiological activities and toxicities in biological systems, efficient chiral separation is essential for enhancing drug efficacy, reducing side effects, and ensuring product safety. Currently, common chiral separation methods include high-performance liquid chromatography,[106] gas chromatography,[107] and crystallization.[108] However, these methods often suffer from limited selectivity, restricted separation efficiency, or complex operation. Therefore, developing highly efficient, tunable, and environmentally friendly chiral separation materials has become a key research focus in this field.

In recent years, POFs have emerged as promising materials for chiral separation due to their highly ordered pore structures, tunable functional groups, and excellent stability. By incorporating chiral recognition sites into the POF framework or constructing chiral microenvironments, efficient enantiomer recognition and selective transport can be achieved, offering new solutions for chiral separation. For example, Ye et al. first reported a cyclodextrin-MOF (CD-MOF) membrane, which was composited with polyvinylidene fluoride (PVDF) via phase inversion–immersion precipitation to fabricate a CD-MOF/PVDF composite membrane for chiral amino acid separation. Under optimized conditions (CD-MOF loading of 5%, polymer concentration of 12%, and casting solution temperature of 70°C), the resulting composite membrane (V-5%–12) exhibited the best performance, achieving a water flux of 466.4 L m^{-2} h, a BSA rejection rate of 24.3%, and stable 100% separation efficiency for phenylalanine (Phe) enantiomers over 4 h. The chiral environment of the membrane was provided by CD-MOF, whose hydrophilicity influenced the membrane's microstructure during the casting process, leading to a specific pore distribution and molecular interactions. This, in turn, regulated the selective transport of chiral molecules, enabling highly efficient chiral separation (**Figure 18**A).[109]

Chen et al. successfully prepared a novel chiral COF membrane (COF/SSCAM) via interfacial polymerization (IP) using TpBD-Am7CD as the chiral functional monomer and TMC as the linking monomer on a stainless steel I-Net cellulose acetate membrane (SSCAM) as the support. The study showed that the introduction of COF containing hydrophilic groups significantly enhanced the membrane's permeability. Moreover, the increase

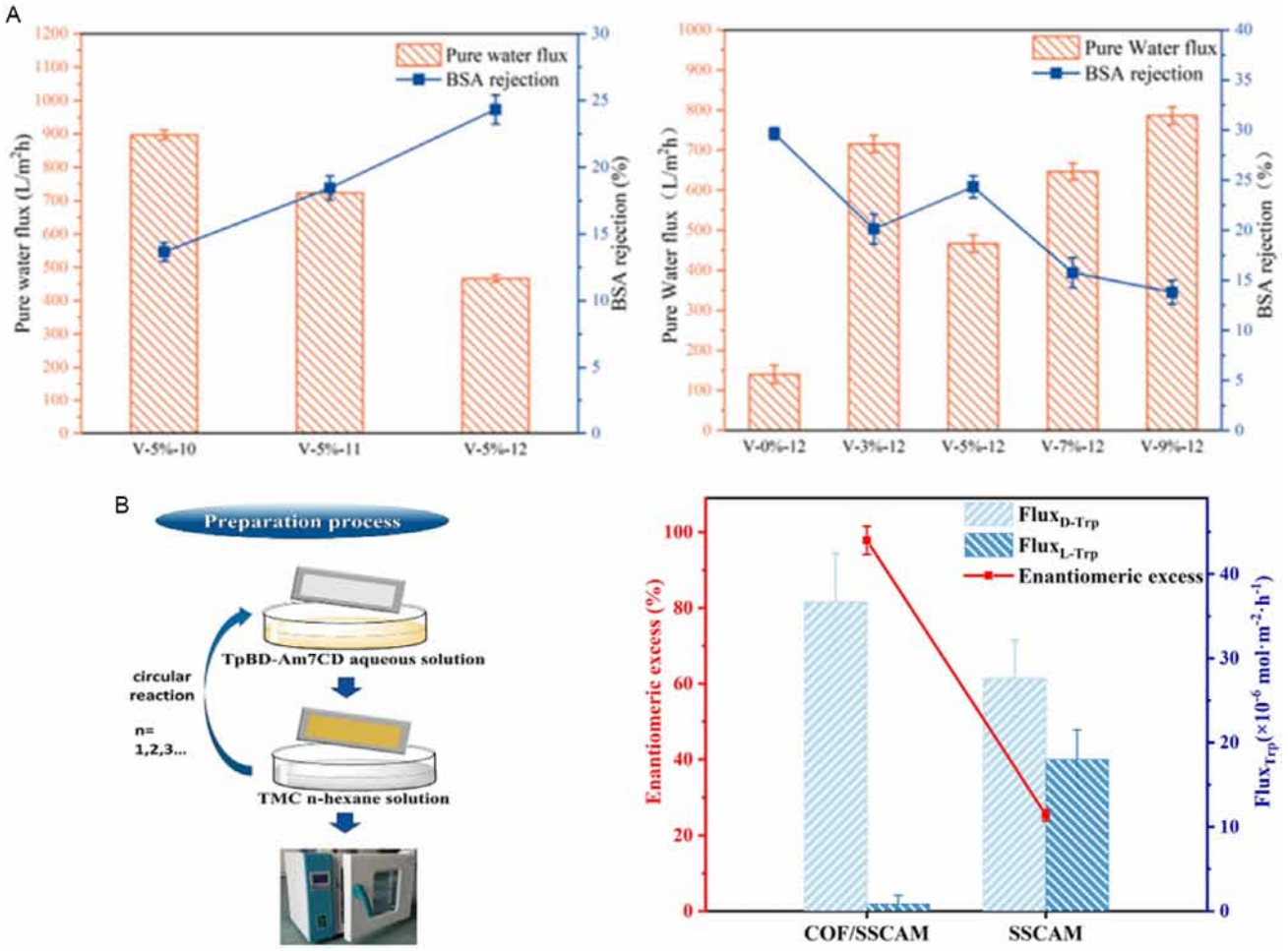

Figure 18. A) Pure water fluxes and BSA rejection rates of V-(0%, 3%, 5%, 7%, 9%)-12, V-5%-(10, 11, 12) (Reproduced with permission.[109] Copyright 2023, Elsevier). B) Schematic of the COF/SSCAM membrane preparation process; enantioselectivity and solute permeation flux of optimal COF/SSCAM and SSCAM for racemic tryptophan (Reproduced with permission.[110] Elsevier, Copyright 2022).

in permeability did not negatively affect the enantioselectivity. Compared to the support membrane SSCAM (enantioselectivity of 25.35%), the COF/SSCAM exhibited superior enantioselectivity (100.00%) for racemic tryptophan, demonstrating excellent separation performance (Figure 18B).[110]

3.3.3. Organic Solvent Separation

Organic solvent separation is an important topic in the fields of chemical engineering and environmental protection, with wide applications in wastewater treatment,[111] petrochemical industry,[112] pharmaceuticals,[113] and fine chemicals.[114] Traditional methods of organic solvent separation, such as distillation[115] and liquid–liquid extraction,[116] are widely used in industry; however, they often suffer from high energy consumption, complex operation, and limited separation efficiency. Therefore, developing efficient, energy-saving, and environmentally friendly separation technologies has become a key focus of current research.

As a new type of functional material, POFs provide an ideal solution due to their tunable pore structures and surface functional groups. POFs can selectively interact with organic solvent molecules, achieving efficient solvent separation. Moreover, the synthesis of POFs is relatively simple, and they exhibit lower energy consumption and higher efficiency during the separation process, offering a more environmentally friendly and efficient alternative technology for organic solvent separation.

For instance, Li et al. easily prepared a 2D Ni-mediated MOF (Ni-MOF) membrane directly from multilayer stacked nanosheets for aqueous and organic molecule separation. The membrane shows reasonable permeability for various organic solvents and exhibits removal rates of 91.37%, 92.01%, and 96.90% for methylene blue, bright yellow, and Evans blue (EB) in isopropanol, respectively. The membrane demonstrates good organic solvent separation performance due to its nanosheets, which were obtained through ultrasonic exfoliation, having appropriate pore structures and high specific surface area, enabling effective molecular sieving (**Figure 19**A).[117]

Xu et al. developed a microwave-assisted method for COF membrane fabrication via in situ polymerization and microwave crystallization. Monomers rapidly polymerized on a porous Al_2O_3 substrate, forming an amorphous precursor that efficiently absorbed microwave energy, accelerating Schiff-base reactions and achieving high crystallinity within 60 min. The resulting COF membrane, with ordered nanopores and excellent stability,

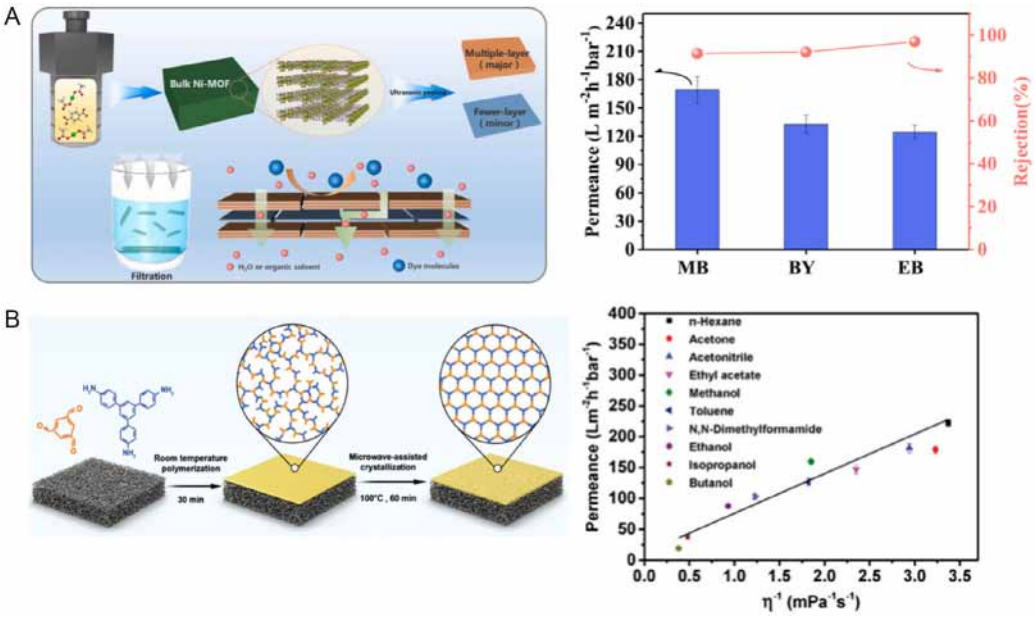

Figure 19. A) Schematic of the fabrication process for the Ni-MOF membranes; separation performance of Ni-MOF membranes for different molecules in isopropyl alcohol (Reproduced with permission.[117] Copyright 2021, Elsevier). B) Schematic illustration of the fabrication process of TFB-TAPB membrane; permeance of organic solvents through TFB-TAPB membrane as a function of their inverse viscosity (Reproduced with permission.[118] Copyright 2024, Wiley).

demonstrated exceptional performance, rejecting 98.7% of EB and exhibiting ethanol and *n*-hexane fluxes of 87.8 and 222.3 L m^{-2} h^{-1} bar^{-1}. Microwave-induced molecular rearrangement enhanced sieving ability, while thermodynamic stability ensured long-term solvent resistance (Figure 19B).[118]

3.3.4. NF

NF is an efficient membrane separation technology widely applied in water treatment, organic solvent separation, and fine chemicals.[119] Its separation mechanism relies on pore size sieving and surface charge effects. However, traditional polymeric or inorganic NF membranes face trade-offs in solvent resistance, mechanical stability, and separation selectivity, making them challenging to meet the demands of extreme environments.[120] POFs, particularly COFs, exhibit great potential in precise molecular sieving and solvent stability due to their tunable pore sizes and excellent stability, offering new opportunities for the development of NF technology.

Han et al. developed a hydrophilic membrane support using THPC-modified COF nanosheets (IL@COF-367 NSs) as an intermediate layer to optimize polyamide membrane properties through interfacial polymerization. The high hydrophilicity and good dispersion of IL@COF-367 NSs facilitated even amine monomer distribution and slowed diffusion to the organic interface. This resulted in an IC-TFN membrane with increased surface roughness (14.5–54.5 nm) and reduced thickness (95–30 nm). The pore size increased from 0.31 to 0.47 nm, leading to a high permeability of 36.5 L m^{-2} h^{-1} bar^{-1} and Na_2SO_4 rejection of 98.5%.[121]

In addition to POF membranes, liquid crystalline nanostructured membranes (LCNMs) represent another promising class of advanced materials for selective separation applications. LCNMs, which are formed by self-assembled liquid crystalline phases, offer unique anisotropic structures that enable precise ion transport and enhanced separation efficiency.[122] For example, Dischinger et al. regulated the filtration performance of ion-type QI-phase lyotropic liquid crystal (LLC) polymer NF membranes with ≈1 nm pores by immersing bicontinuous cubic-phase LLC polymer membranes in a salt solution to promote anion exchange on the pore walls, thereby significantly enhancing pore selectivity and water flux without compromising the structural integrity of the material.[123]

4. Summary and Outlook

Nanostructured POF membranes (MOFs, COFs, and HOFs) have gained widespread applications in various osmotic application including osmotic power conversion, water desalination, and selective separation (**Table 2**), due to their advanced fabrication techniques and excellent selectivity and permeability. The pore sizes of these membranes can be precisely controlled in the angstrom range, perfectly matching the kinetic diameters of ions and small molecules, thereby enabling efficient selective separation. Additionally, the ultrathin nature of the membranes not only reduces mass transfer resistance but also significantly enhances their permeability. These unique properties demonstrate the remarkable advantages of nanostructured POF membranes in osmotic applications, providing a strong foundation for the development of the next generation of ion-selective membranes.

In comparison, while MOF membranes often exhibit superior selectivity due to their tunable pore structures and versatile functionalities, COF membranes stand out for their robust chemical stability and mechanical strength, making them particularly

Table 2. Porous organic framework membranes for osmotic power conversion, seawater desalination, and selective separation.

Membranes	Preparation method	Application	Performance	Ref.
Cu-TCPP	Thermal solvent, sonication	Osmotic power conversion	16.64 W m^{-2}	[78]
PSS/HKUST-1	Encapsulation	Osmotic power conversion	45.6 W m^{-2}	[79]
SP-MIL-53	In situ growth	Osmotic power conversion	8.3 W m^{-2}	[80]
ZnTCPP	Surfactant-assisted	Osmotic power conversion	3.01 W m^{-2}	[56]
UiO-66-NH_2/BANM	In situ solvothermal	Osmotic power conversion	17.1 W m^{-2}	[81]
ZIF-8/PSS@ANM	In situ growth	Osmotic power conversion	23.4 W m^{-2}	[82]
COF-TAPB-BTDA	Liquid–solid interface condensation	Osmotic power conversion	155 W m^{-2}	[83]
COF-TbPa/PAN	Liquid–solid–liquid interface condensation	Osmotic power conversion	20.22 W m^{-2}	[84]
PyPa-SO_3H/SANF	Photografting polymerization	Osmotic power conversion	9.6 W m^{-2}	[85]
ZnTPP-Vg COF	Laminar assembly interfacial polymerization	Osmotic power conversion	102 W m^{-2}	[86]
HOF/AAO	Chemical binding and solution processing	Osmotic power conversion	75.2 W m^{-2}	[43]
UiO-66-NH_2(PSS)/ZIF-8(PVP)	LBL deposition	Osmotic power conversion	40.01 W m^{-2}	[87]
ZIF-8(AAO)/UiO-66-$(COOH)_2$/AAO	Cathodic deposition	Osmotic power conversion	3.44 W m^{-2}	[88]
MOF-303	In situ hydrothermal synthesis	Water desalination	3.0 L m^{-2} h^{-1}·bar^{-1} μm	[89]
UiO-66 MOF	In situ solvothermal synthesis	Water desalination	0.28 L m^{-2} h^{-1}·bar^{-1} μm	[90]
ZIF-8 NPs	Confined interfacial polymerization	Water desalination	>43.6 LMH bar^{-1}	[91]
CONs	Polyelectrolyte-induced biomineralization	Water desalination	341 kg m^{-2} h^{-1}	[92]
COF-$DhTG_{Cl}$	Double-water-phase interfacial assembly	Water desalination	3.7 L m^{-2} h^{-1} bar^{-1}	[64]
TpPa-SO_3H@TpTTPA	Mixed-dimensional strategy	Water desalination	267 kg m^{-2} h^{-1}	[94]
TpPa@PAN-4.0	Electrochemical interfacial polymerization	Water desalination	92 kg m^{-2} h^{-1}	[63]
MOF/organosilica	–	CO_2/CH_4	18.2	[96]
MIL-125	Combining single-mode microwave heating with tertiary growth	CO_2/N_2	38.7	[97]
ACOF-1	Solvothermal	CO_2/CH_4	86.3	[98]
COF-300	Ammonium acetate-assisted steam induction strategy	H_2/CO_2	11	[99]
TP-IQD/6FDA-ODA	Schiff-based condensation	C_2H_2/C_2H_4	11.2	[100]
iCOF@PEI	PMA strategy	CO_2/N_2	33	[101]
UPC-HOF-6	Solution processing method	H_2/N_2	19.5	[102]
HOF-21	Self-assembly process	CO_2/N_2	60	[103]

suitable for harsh operating conditions. On the other hand, HOF membranes have gained attention for their high permeability and ease of synthesis, though they may require further optimization for long-term performance. Recent studies[124] have shown that each type of membrane offers distinct advantages depending on the specific osmotic application, highlighting the need for tailored designs to maximize efficiency in processes such as osmotic power conversion, desalination, and selective separation.

However, despite the numerous advantages that nanostructured POF membranes exhibit in osmotic applications, their future development still faces multiple challenges. First, the long-term stability of the membranes needs to be enhanced to ensure their reliability in practical use. Additionally, optimizing the structure of the membranes to achieve an optimal balance between selectivity and permeability is a key research focus. At the same time, the sustainability and economic viability of commercial production are pressing issues that need to be addressed. The development of membrane materials that balance cost-effectiveness and environmental sustainability has become a key research direction. Future studies should focus on the following several key points: 1) constructing POF membranes with tunable selectively through direct synthesis or chemical modification (such as incorporating different functional groups like —COOH and —NH_2) to enhance selectivity; 2) utilizing various porous materials to create hybrid membranes for improved performance; 3) conducting in-depth study on the relationship between framework structures and osmotic performance; 4) employing advanced computational simulations methods to gain a deeper understanding of the molecular mechanisms of the membranes, thereby guiding material design and improvement; and 5) leveraging machine learning in the synthesis of POFs, as it is essential for optimizing synthesis conditions, predicting material properties, and accelerating the discovery of new materials. By integrating machine learning techniques, the process of designing and discovering efficient POF membranes can be significantly enhanced, ultimately advancing their performance in osmotic applications.[125]

In summary, nanostructured porous organic framework membranes hold great promise for osmotic applications. With the continuous advancement of materials science and nanotechnology,

we anticipate significant breakthroughs in the application of these membranes within the osmotic field. By addressing existing challenges, future research is expected to pave the way for the development of efficient and environmentally friendly osmotic technologies, thereby having a profound impact on sustainable development for humanity.

Acknowledgements

This work was supported by the National Natural Science Foundation (grant no. 22479016).

Conflict of Interest

The authors declare no conflict of interest.

Keywords: covalent organic frameworks · hydrogen-bonded organic frameworks · metal–organic frameworks · nanostructures · osmotic applications

[1] J. R. Werber, C. O. Osuji, M. Elimelech, *Nat. Rev. Mater.* **2016**, *1*, 16018.
[2] D. S. Sholl, R. P. Lively, *Nature* **2016**, *532*, 435.
[3] J. Luo, R. Qiao, B. Ding, *Matter* **2024**, *7*, 3351.
[4] X. Feng, J. Zhu, J. Jin, Y. Wang, Y. Zhang, B. Van der Bruggen, *Prog. Mater. Sci.* **2024**, *144*, 101285.
[5] J. Gu, C. Ren, X. Zong, C. Chen, L. Winnubst, *Ceram. Int.* **2016**, *42*, 12427.
[6] P. Peng, F. Yang, X. Li, S. Li, Z. Wang, *Cell Rep. Phys. Sci.* **2024**, *5*, 101824.
[7] F. Yang, P. Peng, Z.-Y. Yan, H. Fan, X. Li, S. Li, H. Liu, T.-L. Ren, Y. Zhou, Z. L. Wang, D. Wei, *Nat. Energy* **2024**, *9*, 263.
[8] Z. Meng, L. Zhu, X. Wang, M. Zhu, *Acc. Mater. Res.* **2023**, *4*, 180.
[9] P. Y. He, Y. J. Zhang, H. Chen, Z. C. Han, L. C. Liu, *J. Hazard. Mater.* **2020**, *392*, 122359.
[10] L. Yang, L. N. Y. Cao, S. Li, P. Peng, H. Qian, G. Amaratunga, F. Yang, Z. L. Wang, D. Wei, *Nano Energy* **2024**, *129*, 110076.
[11] L. Yang, S. Li, H. Qian, Z. Wang, Z. L. Wang, D. Wei, *MRS Energy Sustain.* **2024**, *11*, 192.
[12] J. Hou, H. Zhang, G. P. Simon, H. Wang, *Adv. Mater.* **2020**, *32*, 1902009.
[13] B. Hosseini Monjezi, K. Kutonova, M. Tsotsalas, S. Henke, A. Knebel, *Angew. Chem. Int. Ed.* **2021**, *60*, 15153.
[14] Z. Zhang, Y. Ye, S. Xiang, B. Chen, *Acc. Chem. Res.* **2022**, *55*, 3752.
[15] Y. Liu, Y. Zhao, X. Zhang, X. Huang, W. Liao, Y. Zhao, *Chem. Eng. J.* **2021**, *422*, 130082.
[16] J. Li, H. Wang, X. Yuan, J. Zhang, J. W. Chew, *Coordin. Chem. Rev.* **2020**, *404*, 213116.
[17] Y. Wang, H. Jin, Q. Ma, K. Mo, H. Mao, A. Feldhoff, X. Cao, Y. Li, F. Pan, Z. Jiang, *Angew. Chem. Int. Ed.* **2020**, *59*, 4365.
[18] L. Ding, Y. Wei, L. Li, T. Zhang, H. Wang, J. Xue, L.-X. Ding, S. Wang, J. Caro, Y. Gogotsi, *Nat. Commun.* **2018**, *9*, 155.
[19] H. Qian, P. Peng, H. Fan, Z. Yang, L. Yang, Y. Zhou, D. Tan, F. Yang, M. Willatzen, G. Amaratunga, Z. Wang, D. Wei, *Angew. Chem. Int. Ed.* **2024**, *63*, e202414984.
[20] P. Peng, H. Qian, J. Liu, Z. Wang, D. Wei, *Int. J. Smart Nano Mater.* **2024**, *15*, 198.
[21] D. Wei, F. Yang, Z. Jiang, Z. Wang, *Nat. Commun.* **2022**, *13*, 4965.
[22] H. Qian, D. Wei, Z. Wang, *Nano Res.* **2023**, *16*, 11718.
[23] P. Peng, F. Yang, Z. Wang, D. Wei, *Adv. Energy Mater.* **2023**, *13*, 2302360.
[24] L. Yang, F. Yang, X. Liu, K. Li, Y. Zhou, Y. Wang, T. Yu, M. Zhong, X. Xu, L. Zhang, W. Shen, D. Wei, *PNAS* **2021**, *118*, e2023164118.
[25] D. Wei, *Sci. Rep.* **2015**, *5*, 15173.
[26] K. Li, W. Shen, T. Xu, L. Yang, X. Xu, F. Yang, L. Zhang, Y. Wang, Y. Zhou, M. Zhong, D. Wei, *Carbon Energ.* **2021**, *3*, 916.
[27] D. Wei, M. R. Astley, N. Harris, R. White, T. Ryhänen, J. Kivioja, *Nanoscale* **2014**, *6*, 9536.
[28] D. Wei, D. Cotton, T. Ryhänen, *Nanomaterials* **2012**, *2*, 268.
[29] N. Gu, D. Wei, L. Niu, A. Ivaska, *Electrochim. Acta* **2006**, *51*, 6038.
[30] F. Zhang, J. Yu, Y. Si, B. Ding, *Adv. Mater.* **2023**, *35*, 2302511.
[31] P. Bernardi, *Nat. Metab.* **2019**, *1*, 752.
[32] J. Li, L. Du, X. Kong, J. Wu, D. Lu, L. Jiang, W. Guo, *Natl. Sci. Rev.* **2023**, *10*, nwad260.
[33] P. Agre, *Angew. Chem. Int. Ed.* **2004**, *43*, 4278.
[34] Y. Li, M. Karimi, Y.-N. Gong, N. Dai, V. Safarifard, H.-L. Jiang, *Matter* **2021**, *4*, 2230.
[35] R. Freund, O. Zaremba, G. Arnauts, R. Ameloot, G. Skorupskii, M. Dincă, A. Bavykina, J. Gascon, A. Ejsmont, J. Goscianska, M. Kalmutzki, U. Lächelt, E. Ploetz, C. S. Diercks, S. Wuttke, *Angew. Chem. Int. Ed.* **2021**, *60*, 23975.
[36] B. Cheng, X. Fu, Y. Song, Z. Li, P. Weng, X. Yin, *Sep. Purif. Technol.* **2024**, *331*, 125701.
[37] W. Zhang, L. Zhang, H. Zhao, B. Li, H. Ma, *J. Mater. Chem. A* **2018**, *6*, 13331.
[38] J. Huang, D. Huang, F. Zeng, L. Ma, Z. Wang, *J. Mater. Sci.* **2021**, *56*, 3127.
[39] I. W. Almanassra, L. Jaber, A. Chatla, A. Abushawish, A. Shanableh, M. Ali Atieh, *Chem. Eng. J.* **2023**, *471*, 144616.
[40] H. Fan, J. Gu, H. Meng, A. Knebel, J. Caro, *Angew. Chem. Int. Ed.* **2018**, *57*, 4083.
[41] C. Yuan, X. Wu, R. Gao, X. Han, Y. Liu, Y. Long, Y. Cui, *J. Am. Chem. Soc.* **2019**, *141*, 20187.
[42] Q. Ye, S.-H. Chen, Y. Zhang, B. Ruan, Y.-J. Zhang, X.-K. Zhang, T. Jiang, X. Wang, N. Ma, F.-C. Tsai, *Macromol. Biosci.* **2021**, *21*, 2100317.
[43] H. Wang, Y. Zhang, J. Wang, Saijilahu, H. Sun, H. Yang, X.-H. Xia, C. Wang, *Adv. Funct. Mater.* **2024**, 2412477.
[44] M. Pandey, K. Deshmukh, A. Raman, A. Asok, S. Appukuttan, G. R. Suman, *Renew. Sustain. Energy Rev.* **2024**, *189*, 114030.
[45] Y.-T. Du, X. Kan, F. Yang, L.-Y. Gan, U. Schwingenschlögl, *ACS Appl. Mater. Interfaces* **2018**, *10*, 32867.
[46] H. Wu, Y. Li, L. Wu, Z. Li, Y. Xing, D. Xiao, Z. Fan, X. Zhang, *Cell Rep. Phys. Sci.* **2024**, *5*, 102035.
[47] V. Chernikova, O. Shekhah, I. Spanopoulos, P. N. Trikalitis, M. Eddaoudi, *Chem. Commun.* **2017**, *53*, 6191.
[48] C. Jiao, X. Song, X. Zhang, L. Sun, H. Jiang, *ACS Appl. Mater. Interfaces* **2021**, *13*, 18380.
[49] J. Campbell, R. P. Davies, D. C. Braddock, A. G. Livingston, *J. Mater. Chem. A* **2015**, *3*, 9668.
[50] J. Wu, Q. Dai, H. Zhang, X. Li, *Energy Storage Mater.* **2021**, *35*, 687.
[51] K. Tulugan, P. Tian, W. Zhao, X. Li, X. Zhang, *Appl. Sci.* **2024**, *14*, 4462.
[52] M. A. Andrés, M. T. Vijjapu, S. G. Surya, O. Shekhah, K. N. Salama, C. Serre, M. Eddaoudi, O. Roubeau, I. Gascón, *ACS Appl. Mater. Interfaces* **2020**, *12*, 4155.
[53] J. C. Espinoza-Tapia, L. A. Becerril-Landero, E. Barrera-Calva, J. G. Vigueras Ramírez, L. González-Reyes, C. Falcony-Guajardo, *Nano Express* **2024**, *5*, 035011.
[54] F. Caddeo, R. Vogt, D. Weil, W. Sigle, M. E. Toimil-Molares, A. W. Maijenburg, *ACS Appl. Mater. Interfaces* **2019**, *11*, 25378.
[55] Y. Xiao, Z. Wu, Q. Zhang, P. Li, H. Yu, G. Lu, *Cryst. Growth Des.* **2020**, *20*, 3997.
[56] Y. Su, J. Hou, C. Zhao, Q. Han, J. Hu, H. Zhang, *J. Mater. Chem. A* **2024**, *12*, 13153.
[57] J. Xiao, M. Cong, M. Li, X. Zhang, Y. Zhang, X. Zhao, W. Lu, Z. Guo, X. Liang, G. Qing, *Adv. Funct. Mater.* **2024**, *34*, 2307996.
[58] H. Li, H. Shi, X. Chen, Z. Ren, Y. Shen, P. Wu, Y. Fan, X. Zhang, W. Shi, H. Liao, S. Zhang, W. Zhang, F. Huo, *Adv. Mater.* **2023**, *35*, 2209777.
[59] C. Huang, C. Liu, X. Chen, Z. Xue, K. Liu, X. Qiao, X. Li, Z. Lu, L. Zhang, Z. Lin, T. Wang, *Adv. Sci.* **2020**, *7*, 1903180.
[60] Q. Wang, Y. Guo, Y. Long, Y. Liu, Z. Wang, Y. Liu, X. Zhang, *J. Membrane Sci.* **2024**, *701*, 122766.
[61] J. E. Lopez-Cazares, K. Kim, J. Y. S. Lin, K. Jin, *Ind. Eng. Chem. Res.* **2024**, *63*, 3684.
[62] W. Deng, Z. Zhang, L. Liu, Z. Zhou, L. Wu, *RSC Adv.* **2024**, *14*, 16510.
[63] M. Wang, Y. Wang, J. Zhao, J. Zou, X. Liang, Z. Zhu, J. Zhu, H. Wang, Y. Wang, F. Pan, Z. Jiang, *Angew. Chem. Int. Ed.* **2023**, *62*, e202219084.
[64] H. Wang, J. Zhao, Y. Li, Y. Cao, Z. Zhu, M. Wang, R. Zhang, F. Pan, Z. Jiang, *Nano-Micro Lett.* **2022**, *14*, 216.
[65] H. Fan, A. Mundstock, A. Feldhoff, A. Knebel, J. Gu, H. Meng, J. Caro, *J. Am. Chem. Soc.* **2018**, *140*, 10094.
[66] M. Chen, K. Yang, J. Wang, H. Sun, X.-H. Xia, C. Wang, *Adv. Funct. Mater.* **2023**, *33*, 2302427.
[67] M. Chen, M. Trubyanov, P. Zhang, D. Rodríguez-San-Miguel, F. Zamora, K. S. Novoselov, D. V. Andreeva, *Carbon* **2024**, *219*, 118855.
[68] C. Zhang, T. Xiao, J. He, B. Lu, X. Li, J. Zhai, X. Fan, *Small* **2023**, *19*, 2301512.
[69] H. Zeng, C. Yao, C. Wu, D. Wang, W. Ma, J. Wang, *Small* **2024**, *20*, 2310811.
[70] J.-f. Feng, T.-F. Liu, R. Cao, *Angew. Chem. Int. Ed* **2020**, *59*, 22392.

[71] C. Zhang, Z. Wang, L. Qiao, L. Yu, J. Pang, Y. Feng, W. Chen, L. Fan, R. Wang, H. Guo, Z. Kang, D. Sun, *Angew. Chem. Int. Ed.* **2024**, *63*, e202407779.
[72] Y. Liu, H. Wu, R. Li, J. Wang, Y. Kong, Z. Guo, H. Jiang, Y. Ren, Y. Pu, X. Liang, F. Pan, Y. Cao, S. Song, G. He, Z. Jiang, *Adv. Mater.* **2022**, *34*, 2201423.
[73] J. Fu, S. Das, G. Xing, T. Ben, V. Valtchev, S. Qiu, *J. Am. Chem. Soc.* **2016**, *138*, 7673.
[74] X. Ma, N. Sun, Z. Li, M. Tong, Q. Ding, Z. Wang, L. Bai, L. Dong, Y. Liu, *Adv. Funct. Mater.* **2024**, *34*, 2312203.
[75] T. Xu, B. Wu, W. Li, Y. Li, Y. Zhu, F. Sheng, Q. Li, L. Ge, X. Li, H. Wang, T. Xu, *Sci. Adv.* **2024**, *10*, eadn0944.
[76] X. Zhang, S. Xin, Q. Qian, X. Xi, M. Fang, Z. Sun, Y. Wang, Y. Li, Y. Wang, X. Tian, Y. Li, S. Wang, J. Yang, Z. Tang, L. Li, *NPG Asia Mater.* **2025**, *17*, 1.
[77] X.-T. Bai, L.-H. Cao, X.-Y. Chen, J.-Y. Wang, Z.-Y. Zhou, *Sci. China-Chem.* **2025**, 1.
[78] J. Wang, Z. Song, M. He, Y. Qian, D. Wang, Z. Cui, Y. Feng, S. Li, B. Huang, X. Kong, J. Han, L. Wang, *Nat. Commun.* **2024**, *15*, 2125.
[79] S. Pan, P. Liu, Q. Li, B. Zhu, X. Liu, J. Lao, J. Gao, L. Jiang, *Angew. Chem. Int. Ed.* **2023**, *62*, e202218129.
[80] Y. Liu, Y. Chen, Y. Guo, X. Wang, S. Ding, X. Sun, H. Wang, Y. Zhu, L. Jiang, *ACS Nano* **2022**, *16*, 16343.
[81] Z.-J. Yang, L.-H. Yeh, Y.-H. Peng, Y.-P. Chuang, K. C. W. Wu, *Angew. Chem. Int. Ed.* **2024**, *63*, e202408375.
[82] A. R. Fauziah, C.-W. Chu, L.-H. Yeh, *Chem. Eng. J.* **2023**, *452*, 139244.
[83] Z. Lai, Y. Ai, W. Xian, Q. Guo, Q.-W. Meng, S. Yin, S. Wang, L. Zhang, Y. Xiong, B. Chen, Q. Sun, *Adv. Funct. Mater.* **2024**, 2409356.
[84] S. Yin, J. Li, Z. Lai, Q.-W. Meng, W. Xian, Z. Dai, S. Wang, L. Zhang, Y. Xiong, S. Ma, Q. Sun, *Nat. Commun.* **2024**, *15*, 8137.
[85] Z. Man, J. Safaei, Z. Zhang, Y. Wang, D. Zhou, P. Li, X. Zhang, L. Jiang, G. Wang, *J. Am. Chem. Soc.* **2021**, *143*, 16206.
[86] Z. Huang, M. Fang, B. Tu, J. Yang, Z. Yan, H. G. Alemayehu, Z. Tang, L. Li, *ACS Nano* **2022**, *16*, 17149.
[87] R. K. Tonnah, M. Chai, M. Abdollahzadeh, H. Xiao, M. Mohammad, E. Hosseini, M. Zakertabrizi, D. Jarrahbashi, A. Asadi, A. Razmjou, M. Asadnia, *ACS Nano* **2023**, *17*, 12445.
[88] Z.-Q. Li, G.-L. Zhu, R.-J. Mo, M.-Y. Wu, X.-L. Ding, L.-Q. Huang, Z.-Q. Wu, X.-H. Xia, *ACS Appl. Mater. Interfaces* **2023**, *15*, 23922.
[89] S. Cong, Y. Yuan, J. Wang, Z. Wang, F. Kapteijn, X. Liu, *J. Am. Chem. Soc.* **2021**, *143*, 20055.
[90] X. Liu, N. K. Demir, Z. Wu, K. Li, *J. Am. Chem. Soc.* **2015**, *137*, 6999.
[91] H. You, W. Luo, P. Chammingkwan, T. Taniike, *Sep. Purif. Technol.* **2024**, *351*, 128126.
[92] Z. Wang, J. Qi, X. Lu, H. Jiang, P. Wang, M. He, J. Ma, *J. Membrane Sci.* **2021**, *630*, 119327.
[93] J. Zhao, Y. Wang, Z. Zhang, Z. Zhu, S. Zeng, G. Yang, S. Zhang, F. Pan, Z. Jiang, *Small* **2024**, *20*, 2310566.
[94] M. Wang, P. Zhang, X. Liang, J. Zhao, Y. Liu, Y. Cao, H. Wang, Y. Chen, Z. Zhang, F. Pan, Z. Zhang, Z. Jiang, *Nat. Sustain.* **2022**, *5*, 518.
[95] A. Roevens, J. G. Van Dijck, D. Geldof, F. Blockhuys, B. Prelot, J. Zajac, V. Meynen, *Appl. Surf. Sci.* **2017**, *416*, 716.
[96] C. Kong, H. Du, L. Chen, B. Chen, *Energ. Environ. Sci.* **2017**, *10*, 1812.
[97] C. Wang, Y. Sun, L. Li, R. Krishna, T. Ji, S. Chen, J. Yan, Y. Liu, *Angew. Chem. Int. Ed.* **2022**, *61*, e202203663.
[98] H. Fan, A. Mundstock, J. Gu, H. Meng, J. Caro, *J. Mater. Chem. A* **2018**, *6*, 16849.
[99] B. Li, Z. Wang, Z. Gao, J. Suo, M. Xue, Y. Yan, V. Valtchev, S. Qiu, Q. Fang, *Adv. Funct. Mater.* **2023**, *33*, 2300219.
[100] J. Li, Z. Cheng, Z. Wang, J. Dong, H. Jiang, W. Wang, X. Zou, G. Zhu, *Angew. Chem. Int. Ed.* **2023**, *62*, e202216675.
[101] S. Wang, Y. Yang, X. Liang, Y. Ren, H. Ma, Z. Zhu, J. Wang, S. Zeng, S. Song, X. Wang, Y. Han, G. He, Z. Jiang, *Adv. Funct. Mater.* **2023**, *33*, 2300386.
[102] S. Feng, Y. Shang, Z. Wang, Z. Kang, R. Wang, J. Jiang, L. Fan, W. Fan, Z. Liu, G. Kong, Y. Feng, S. Hu, H. Guo, D. Sun, *Angew. Chem. Int. Ed.* **2020**, *59*, 3840.
[103] Y. Wang, Y. Ren, Y. Cao, X. Liang, G. He, H. Ma, H. Dong, X. Fang, F. Pan, Z. Jiang, *Nano-Micro Lett.* **2023**, *15*, 50.
[104] C. Yu, B. H. Yin, Y. Wang, S. Luo, X. Wang, *Coord. Chem. Rev.* **2023**, *495*, 215392.
[105] T. Liu, Z. Li, J. Wang, J. Chen, M. Guan, H. Qiu, *Chem. Eng. J.* **2021**, *410*, 128247.
[106] C. Liu, K. Quan, J. Chen, X. Shi, H. Qiu, *J. Chromatogr. A* **2023**, *1700*, 464032.
[107] Z. Wang, W. Wang, L. Sun, B. Tang, F. Zhang, A. Luo, *J. Chromatogr. A* **2023**, *1702*, 464100.
[108] K. A. Borchardt-Setter, L. Yu, *Cryst. Growth Des.* **2023**, *23*, 3615.
[109] Q. Ye, J. Li, Y. Huang, H. Wu, Y. Li, B. Yan, *J. Environ. Chem. Eng.* **2023**, *11*, 109250.
[110] W. Chen, H. Liu, Y. Chen, J. Ke, X. Qiu, J. Chen, Y. Ji, *Sep. Purif. Technol.* **2023**, *323*, 124406.
[111] L. Zhang, X. Tang, J. Li, G. Deng, M. Yao, F. Yang, *Microchem. J.* **2024**, *205*, 111295.
[112] Y. Feliachi, A. Roy, Y. Ren, M. G. Finn, R. P. Lively, *J. Membrane Sci.* **2024**, *695*, 122462.
[113] B. Alhazmi, G. Ignacz, M. Di Vincenzo, M. N. Hedhili, G. Szekely, S. P. Nunes., *Nat. Commun.* **2024**, *15*, 7151.
[114] D. Wei, T. Lindfors, C. Kvarnström, L. Kronberg, R. Sjöholm, A. Ivaska, *JEAC* **2005**, *575*, 19.
[115] H. Sui, C. Tian, H. Deng, Z. Ming, Z. Zhang, W. Fu, J. Li, *Sep. Purif. Technol.* **2025**, *357*, 130019.
[116] K. Yanagisawa, M. Harada, T. Okada, *ACS Sustainable Chem. Eng.* **2018**, *6*, 10120.
[117] G. Li, Y. Qi, H. Lin, N. Lu, J. Chen, J. Wang, Q. Han, F. Liu, *J. Membrane Sci.* **2021**, *635*, 119470.
[118] K. Xu, Y. Zheng, J. Zhou, Y. Zhao, X. Pang, L. Cheng, H. Wang, X. Zhang, R. Zhang, Z. Jiang, *Adv. Funct. Mater.* **2024**, *12*, 2417383.
[119] D. Yadav, S. Karki, P. G. Ingole, *J. Environ. Chem. Eng.* **2022**, *10*, 108109.
[120] S. M. S, T. Elmakki, S. Zavahir, H. Tariq, A. Abdulhameed, H. Park, H. K. Shon, D. S. Han, *Desalination* **2024**, *592*, 118148.
[121] S. Han, W. You, S. Lv, C. Du, X. Zhang, E. Zhang, J. Zhu, Y. Zhang, *Desalination* **2023**, *548*, 116300.
[122] D. Devadiga, A. T. N., *Adv. Mater. Interfaces* **2022**, *9*, 2101276.
[123] S. M. Dischinger, M. J. McGrath, K. R. Bourland, R. D. Noble, D. L. Gin, *J. Membrane Sci.* **2017**, *529*, 72.
[124] G. Fadillah, N. T. S. Alarifi, I. W. K. Suryawan, T. A. Saleh, *J. Water Process Eng.* **2024**, *63*, 105417.
[125] H. Park, X. Yan, R. Zhu, E. A. Huerta, S. Chaudhuri, D. Cooper, I. Foster, E. Tajkhorshid, *Commun. Chem.* **2024**, *7*, 21.

Manuscript received: November 25, 2024
Revised manuscript received: March 18, 2025
Version of record online: March 23, 2025